arXiv:astro-ph/0607084v3 27 May 2007

Goodness-of-Fit Tests DIFF1 and DIFF2 for Locally-Normalized Supernova Spectra

David J. Jeffery[1], Wesley Ketchum[1], David Branch[1], E. Baron[1], Abouazza Elmhamdi[2,3], & I.J. Danziger[3]

ABSTRACT

Two quantitative tests DIFF1 and DIFF2 for measuring goodness-of-fit between two locally-normalized supernova spectra are presented. Locally-normalized spectra are obtained by dividing a spectrum by the same spectrum smoothed over a wavelength interval relatively large compared to line features, but relatively small compared to continuum features. DIFF1 essentially measures the mean relative difference between the line patterns of locally-normalized spectra and DIFF2 is DIFF1 minimized by a relative logarithmic wavelength shift between the spectra: the shift is effectively an artificial relative Doppler shift. Both DIFF1 and DIFF2 measure the physical similarity of line formation, and thus of supernovae. DIFF1 puts more weight on overall physical similarity of the supernovae than DIFF2 because the DIFF2 shift compensates somewhat for some physical distinction in the supernovae. Both tests are useful in ordering supernovae into empirical groupings for further analysis. We present some examples of locally-normalized spectra for Type IIb supernova SN 1993J with some analysis of these spectra. The UV parts of two of the SN 1993J spectra are *HST* spectra that have not been published before. We also give an example of fitted locally-normalized spectra and, as an example of the utility of DIFF1 and DIFF2, some preliminary statistical results for hydrogen-deficient core-collapse (HDCC) supernova spectra. This paper makes use of and refers to material to found at the first author's online supernova spectrum database SUSPEND (SUpernovae Spectra PENDing further analysis).[1]

Subject headings: methods: data analysis — supernovae: general — supernovae: individual (SN 1987K, SN 1993J)

[1]Homer L. Dodge Department of Physics & Astronomy, University of Oklahoma, 440 W. Brooks St., Norman, Oklahoma 73019, U.S.A.

[2]ICTP- The International Centre for theoretical Physics, Strada Costiera 11 34014, Trieste, Italy

[3]INAF-Osservatorio Astronomico di Trieste, via G.B. Tiepolo 11, 34131 Trieste, Italy

[1]See http://www.nhn.ou.edu/~jeffery/astro/sne/spectra/spectra.html .

1. INTRODUCTION

An ordinary χ^2-like test measuring the goodness-of-fit of two supernova spectra often fails to be consistent with what the eye sees qualitatively: good agreement to the eye can be poor or moderate agreement by a χ^2-like test. Since the human eye is an excellent pattern recognization tool, judgments based on eye comparisons informed by a specialist's understanding of spectrum formation are often preferred over χ^2-like tests or other formulaic tests in identifying similarity and/or goodness-of-fit between two spectra. Human judgment, of course, is qualitative and to some degree subjective. Thus, it would be advantageous to have tests that measure spectrum similarity more consistently with what the eye sees and yet be quantitative and objective. Such tests could be applied in an automated fashion and, one hopes, would show correlations missed by the eye.

In this paper, we present two quantitative tests DIFF1 and DIFF2 for measuring goodness-of-fit between two supernova spectra. The tests are both measures of the relative difference in line patterns. (The formulae for DIFF1 and DIFF2 are given, respectively, in §§ 4.1 and 4.2.) Both tests depend on what we call local normalization which largely removes continuum features without distorting the line features too much. Local normalization reduces the continuum shape to an apparent flat line of height 1 by dividing the original spectrum by a version of the spectrum smoothed over wavelength interval relatively large compared to line features, but relatively small compared to continuum features. Ordinary (or global) normalization is just to divide the spectrum by a constant chosen for some purpose. The near-equivalent of local normalization has frequently been used for synthetic spectrum calculations simply by inputting a flat continuum at the base of a model atmosphere or by dividing a synthetic spectrum by a known continuum. In the context of synthetic supernova spectra see, e.g., Dessart & Hillier (2005) for this kind of procedure. But note that local normalization is a particular procedure applied to spectra with line features and it cannot be exactly equivalent to using a flat continuum or dividing a spectrum by a known continuum in synthetic spectrum calculations.

DIFF1 and DIFF2 evolved from the DIFF test presented by Branch et al. (2006b). DIFF1 essentially measures the mean relative difference between the line patterns of locally-normalized spectra and DIFF2 is DIFF1 minimized by a relative logarithmic wavelength shift between the spectra: the shift is effectively an artificial relative Doppler shift. From this description, the reader can roughly understand both tests before knowing the test formulae. Both DIFF1 and DIFF2 measure the physical similarity of line formation, and thus of supernovae. DIFF1 puts more weight on overall physical similarity of the supernovae than DIFF2 because the DIFF2 shift compensates somewhat for some physical distinction in the supernovae. Both tests are useful in ordering supernovae into empirical groupings for further

analysis.[2]

There are several reasons for local normalization (or some similar continuum elimination technique) in comparative supernova spectrum analysis. First, the intrinsic supernova continuum can often be quite uncertain. Often the main reason for this is uncertainty in the reddening correction. Error in reddening correction can affect, for example, the $B-V$ color and other colors (particularly toward the blue) by a significant fraction of a magnitude or more. Uncertainty in reddening is particularly a problem for core-collapse supernovae (i.e., Types II-P, II-L, IIn, IIb, Ib, Ic, and Ic hypernovae) which tend to arise in or near star-forming regions in their host galaxies. Foreground Galactic reddening can be reasonably confidently corrected for using the results of Schlegel et al. (1998) for Galactic reddening and Cardelli et al. (1989) and O'Donnell (1994) for the reddening law, but the host galaxy reddening can usually only be corrected for with great uncertainty relying on interstellar lines in the supernova spectra or, with less uncertainty depending on cases, on spectral modeling. For example, early spectral modeling of Type II-P supernovae can constrain reddening (Baron et al. 2003, 2004, 2005). Nevertheless, in spectral modeling one would much prefer to have reddening as a given rather than as a parameter to be fitted for—or not to be a consideration which is what local normalization helps toward. Core-collapse supernova types are all rather heterogeneous types, and so judging reddening by a comparison of a supernova to other examples of its type is not usually conclusive. Type Ia supernovae (SNe Ia) are usually much less reddened as they do not preferentially arise in or near star forming regions and the homogeneity of most of them (e.g., Branch et al. 2006b) allows reddening correction by comparison in some cases. But even SNe Ia can be highly reddened (e.g., SN 1986G (Phillips et al. 1987)) and there are peculiar SNe Ia (e.g., Branch et al. 2006b) for which comparisons to determine reddening can be uncertain. Thus, the reddening correction for SNe Ia is often uncertain.

In addition to reddening, the continuum can be in error because of errors in the broad-band calibration of the spectrum. A particular problem in achieving good calibration arises because supernovae are transient, time-dependent sources: this means one usually cannot simply replace a bad observation by a good one for a given epoch and this limits the ability to achieve good calibration. Another related particular problem arises from the fact that bright well-observed supernovae are relatively rare. Thus, many well-observed supernovae are from

[2]While this paper was in preparation, analysis tools for supernova spectra that are in some respects similar to DIFF1 and DIFF2 with local normalization were described by Stéphane Blondin (Blondin & Tonry 2007) and Avet Harutyunyan (Harutyunyan et al. 2005) at the conference *The Multi-coloured Landscape of Compact Objects and their Explosive Origins*, Cefalù, Sicily, 2006 June 11–24, URL: http://www.mporzio.astro.it/cefalu2006/ .

earlier instrumentation epochs. One would like to use the data from these supernovae for analysis since they are to some degree unique even though the data may have very uncertain calibration by modern standards.

Reddening and calibration errors tend to affect the spectrum continuum multiplicatively: i.e., they change flux level by a scaling factor that varies slowly with wavelength. These kind of uncertainties are ideally, and nearly practically, irrelevant to the process of local normalization (see § 2.1), and thus cannot much affect analysis with the locally-normalized spectra.

A kind of continuum uncertainty that is not eliminated by local normalization is the additive uncertainty due to contamination by extraneous sources. (See § 2.1 for why this is so.) The most common contamination is from the host galaxy emission. When a supernova is at its brightest this contamination is often small, but in later phases when the supernova dims it can become significant and dominant. Host galaxy contamination can be subtracted off using spectra of the galaxy when the supernovae is absent, but it is not always clear to analyzers of supernova spectra when this has been done. Another kind of contamination is peculiar to supernovae associated with gamma-ray bursts (GRBs): such supernovae may all be what are now called hypernovae (since they are very energetic and perhaps very massive) or as we prefer Type Ic hypernovae since they seem to lack conspicuous lines of hydrogen and helium and the strong Si II λ6355 line. (Lack of conspicuous hydrogen and helium lines together with the lack of a strong Si II λ6355 line are the defining observational characteristics of Type Ic supernovae.) The contamination is the UVOIR (ultraviolet-optical-infrared) afterglow of the GRB itself which tends to be a line-free continuum. Correction for this kind of contamination can be done, but with some uncertainty (Matheson et al. 2003). Yet another contamination (which unfortunately also affects the line pattern) is light echoing caused by supernova light from earlier phases reflected off dust clouds and added to the light of the current supernova phase. Light echoes, if recognized, can be corrected for, but with some error, of course. For the developments in this paper, we assume that contamination of all kinds can be adequately corrected for.

Because of all the effects mentioned above, the continuum shape of supernova spectra may be incorrect and misleading about the degree of similarity between spectrum pairs. On the other hand the line pattern in the spectra should be better for determining similarities since this is less affected by broad-band uncertainties in reddening and calibration. For example, if a spectrum pair had an identical line pattern, but different continuum shapes, one would have good reason to believe that the supernovae are, in fact, highly similar and at a similar phase in their evolution and that the discrepancy in continuum shape was just caused by reddening correction and/or calibration error. In the contrasting case, where the

line patterns are very different, but the continuum shapes are identical, one would conclude the supernovae are not very similar or at different phases in their evolution despite the similar continua. In both extreme cases, it is the line patterns that provide the decisive evidence, not the continua. Thus, if one can adequately correct or neglect contamination, analysis with locally-normalized spectra should give good insight into the intrinsic similarities and differences among supernovae. It is a basic premise of this paper that line pattern is a much better signature of intrinsic supernova behavior than continuum shape, and so eliminating continuum shape information is not too important for spectrum comparisons.

A second reason for using local normalization applies even when the continuum shapes are assumed to be well known. If one is searching just for similarity of line patterns as a clue to physical similarities, then varying continuum shapes tend to obscure the similarities of the patterns both to the eye and formulaic tests. Being able to measure similarity of line patterns for heterogeneous samples of supernovae from varying phases is important in studying the time-varying supernova structure. Especially for core-collapse supernovae in which even members of the same type show considerably individuality and in which the time coverage of their evolution can often be very incomplete, local normalization could become an important tool in analysis.

A third reason, for local normalization is that spectra are frequently analyzed using synthetic spectra calculated from highly simplified radiative transfer: e.g., analyses done using the parameterized code SYNOW (e.g., Branch et al. 2003, 2005, and references therein) Such simplified radiative transfer does not treat continuum radiative transfer with high physical realism and in fits of synthetic to observed spectra mismatches in the continuum in some regions are obvious and are not considered very important in the important results derived from the synthetic spectrum analysis: the important results being line identification and ejecta velocity structure. Local normalization of both observed and synthetic spectra can be used to reduce the distraction of mismatching continuum shapes (e.g., Parrent et al. 2007).

In § 2 of this paper, we discuss the theoretical basis for local normalization and how we actually carry out local normalization. Section 3 gives examples of locally-normalized spectra for the Type IIb supernova SN 1993J with some analysis of these spectra. The UV parts of two of the SN 1993J spectra are *Hubble Space Telescope* (*HST*) spectra that have not been published before. Also in § 3 (§ 3.5) is an investigation of the continuum independence of local normalization. The DIFF1 and DIFF2 formulae are presented in § 4, where we also present an example of fitted locally-normalized spectra. As an example of the utility of DIFF1/2, § 5 gives some preliminary statistical results for the spectra of supernovae of Types IIb, Ib, Ic, and Ic hypernovae. We will collectively refer to these supernovae as

hydrogen-deficient core-collapse (HDCC) supernovae. Conclusions and discussion are given in § 6.

This paper makes use of and refers to material found at the first author's online supernova spectrum database SUSPEND (SUpernovae Spectra PENDing further analysis). The URL for SUSPEND is given in a footnote to the abstract.

2. LOCAL NORMALIZATION

The basic procedure of local normalization is to divide a spectrum by a smoothed version of itself where the smoothing length is sufficiently large that line features are largely erased, but the continuum shape is largely unaffected, in the smoothed version. We call the smoothing for local-normalization large-scale smoothing to distinguish it from the small-scale smoothing used to suppress noise. The spectrum resulting from the division has ideally a continuum level of 1 everywhere as judged by the eye.

In § 2.1, we discuss the theoretical basis for local normalization. In § 2.2, we discuss our actual procedure for carrying out local normalization.

2.1. The Theoretical Basis for Local Normalization

For concreteness, in our discussion let us model an observed spectrum $f_{\lambda,\mathrm{obs}}$ by the following heuristic formula:

$$f_{\lambda,\mathrm{obs}} = S_\lambda f_{\lambda,\mathrm{con}} f_{\lambda,\mathrm{lin}} + C_\lambda \ , \tag{1}$$

where S_λ is some kind of multiplicative scaling error which could be the effect of unknown reddening or calibration error, $f_{\lambda,\mathrm{con}}$ is the intrinsic continuum spectrum, $f_{\lambda,\mathrm{lin}}$ is the line spectrum, C_λ is some extraneous and unknown contamination flux, and

$$f_{\lambda,\mathrm{int}} = f_{\lambda,\mathrm{con}} f_{\lambda,\mathrm{lin}} \ , \tag{2}$$

is the intrinsic spectrum. The line spectrum is defined by saying it has a height of 1 when it is smoothed over some specified smoothing length that is of order the size of the full width of an individual line profile: thus

$$\langle f_{\lambda,\mathrm{lin}} \rangle = 1 \ , \tag{3}$$

where the angle brackets indicate smoothing with the required smoothing length. We make the assumption that S_λ, $f_{\lambda,\mathrm{con}}$, and C_λ are all sufficiently slowly varying with wavelength that smoothing them over the smoothing length leaves them effectively unchanged. (We are

neglecting the possibility of uncorrected-for light-echo contamination (see § 1).) Now say we smooth the observed spectrum over the smoothing length. We obtain

$$\langle f_{\lambda,\mathrm{obs}} \rangle = \langle S_\lambda f_{\lambda,\mathrm{con}} f_{\lambda,\mathrm{lin}} \rangle + C_\lambda \ , \tag{4}$$

where we have used the assumption that C_λ is unaffected by smoothing. Assuming that $S_\lambda f_{\lambda,\mathrm{con}}$ can be approximated as constant over line widths, we now obtain

$$\langle S_\lambda f_{\lambda,\mathrm{con}} f_{\lambda,\mathrm{lin}} \rangle = \langle S_\lambda f_{\lambda,\mathrm{con}} \rangle \langle f_{\lambda,\mathrm{lin}} \rangle = S_\lambda f_{\lambda,\mathrm{con}} \ , \tag{5}$$

where we have used the assumptions that S_λ and $f_{\lambda,\mathrm{con}}$ are unaffected by smoothing and equation (3). Making use of equations (1), (4), and (5), and our concept of local normalization, the locally-normalized version of $f_{\lambda,\mathrm{obs}}$ (which we denote by $f_{\lambda,\mathrm{LN}}$) is given by

$$f_{\lambda,\mathrm{LN}} = \frac{f_{\lambda,\mathrm{obs}}}{\langle f_{\lambda,\mathrm{obs}} \rangle} = \frac{S_\lambda f_{\lambda,\mathrm{con}} f_{\lambda,\mathrm{lin}} + C_\lambda}{S_\lambda f_{\lambda,\mathrm{con}} + C_\lambda} = f_{\lambda,\mathrm{lin}} \left[\frac{1 + C_\lambda / (S_\lambda f_{\lambda,\mathrm{con}} f_{\lambda,\mathrm{lin}})}{1 + C_\lambda / (S_\lambda f_{\lambda,\mathrm{con}})} \right] \ . \tag{6}$$

What we would really like to have is the line spectrum $f_{\lambda,\mathrm{lin}}$ (as we have defined it above) and what we can obtain from measurements is $f_{\lambda,\mathrm{LN}}$. The line spectrum $f_{\lambda,\mathrm{lin}}$ is what we believe contains much of the information about the object that we are interested in. The $f_{\lambda,\mathrm{lin}}$ and $f_{\lambda,\mathrm{LN}}$ spectra are equal if contamination is zero no matter what S_λ and $f_{\lambda,\mathrm{con}}$ may be given our assumptions. (The equality is only exact in the spectrum model of this discussion. In reality, it can only be approximate since line and continuum behavior cannot be completely separated.) Thus, the effect of any scaling errors are eliminated from the locally-normalized spectra in the absence of contamination. This is one of the great benefits of using locally-normalized spectra in spectrum analysis.

If $C_\lambda / (S_\lambda f_{\lambda,\mathrm{con}}) << 1$ and $f_{\lambda,\mathrm{lin}}$ not much smaller than 1, then

$$f_{\lambda,\mathrm{LN}} \approx f_{\lambda,\mathrm{lin}} \left[1 + \frac{C_\lambda}{S_\lambda f_{\lambda,\mathrm{con}}} \left(\frac{1}{f_{\lambda,\mathrm{lin}}} - 1 \right) \right] \ , \tag{7}$$

where we have expanded equation (6) to first order in $C_\lambda / (S_\lambda f_{\lambda,\mathrm{con}})$. We see that contamination error only cancels to zeroth order. Nevertheless, if $C_\lambda / (S_\lambda f_{\lambda,\mathrm{con}})$ is sufficiently small, then contamination will have only a small effect on the locally-normalized spectrum. On the other hand, if $C_\lambda / (S_\lambda f_{\lambda,\mathrm{con}})$ becomes large compared to 1 and $f_{\lambda,\mathrm{lin}}$, the locally-normalized spectrum tends to have value 1 everywhere and be almost independent of the line spectrum as one can see from equation (6).

In the rest of this paper, we assume contamination is, in fact, negligible or has been adequately corrected for, and thus that C_λ is approximately zero. Given this assumption, the locally-normalized spectra are approximately the line spectra as we have defined them above.

2.2. The Procedure of Carrying Out Local Normalization

There is probably no absolute optimum way of carrying out the basic procedure of local normalization. We have developed a prescription, however, that seems very adequate. The large-scale smoothing is box-car-like where we march through the spectrum wavelength by wavelength and make use of a box-car interval about each wavelength to construct a smoothed flux value at that wavelength. The size of the box-car interval is the smoothing length.

The choice of the smoothing length is a key point. If one makes the smoothing length too small, line features tend to get suppressed in the locally-normalized spectra: in the limit that the smoothing length goes to zero, the locally-normalized spectra become 1 everywhere. On the other hand, if one makes the smoothing length too large, then the locally-normalized spectra retain continuum features: in the limit that the smoothing length goes to infinity, the locally-normalized spectra are just ordinary (or globally) normalized spectra. Unfortunately in supernova spectra, the wavelength scale of the P Cygni and emission line profiles can be very large because of the large Doppler shift velocities in the supernova ejecta. (Supernova lines in the photospheric or optically-thick phase are broad P-Cygni lines with a blueshifted absorption and an emission feature centered roughly on the rest-frame line-center wavelength. See, e.g., Jeffery & Branch (1990, p. 173–194) for a discussion of P-Cygni line formation in supernovae.) Usually, the largest velocities one needs to consider are of order $30,000\,\mathrm{km\,s^{-1}}$ and these lead to relative Doppler shifts of line opacity wavelength of $v/c \sim 0.1$ or of order 10 %. However, line features can form at velocities of up to perhaps $50,000\,\mathrm{km\,s^{-1}}$ in Type Ic hypernovae (e.g., Mazzali et al. 2000) at early times and of up to at least $40,000\,\mathrm{km\,s^{-1}}$ in other kinds of supernovae if seen at sufficiently early times in the UV as evidenced by the P Cygni line of the resonance multiplet Mg II λ2797.9 (e.g., Wiese et al. 1969, p. 30; Moore & Merrill 1968, p. 10) seen in the earliest *IUE* spectrum of Type II supernova SN 1987A (e.g., Pun et al. 1995). With Doppler shift velocity of $50,000\,\mathrm{km\,s^{-1}}$, a relative wavelength shift would be $v/c \sim 1/6$ or of order 17 %. Since one has to consider opacity shifted both to the blue and the red, the relative wavelength width of a line profile in extreme cases could be of order 34 %. Continuum features that vary on the scale of 34 % of wavelength certainly exist. Thus, for supernovae at least in extreme cases, one cannot completely decouple line and continuum behavior.

One must make a choice for the smoothing length for locally-normalized spectra that does not suppress line behavior too much and that does not let too much continuum behavior leak in. There is probably no absolute optimum choice for all cases. We have found that a relative smoothing length of 30 % of the current wavelength in the smoothing procedure is good: the smoothing region extends 15 % blueward and 15 % redward of the current wavelength

as one marches through the wavelength points. The choice of 30 % is motivated as follows. The continuum level determined by blackbody-behavior and reddening (Cardelli et al. 1989; O'Donnell 1994) is relatively constant over a region of 30 % surrounding a wavelength. On the other hand, as mentioned above, usually the largest velocities one needs to consider are of order $30,000\,\mathrm{km\,s^{-1}}$ and these lead to relative Doppler shifts of line opacity wavelength of $v/c \sim 0.1$ or of order 10 %: the whole line profile in this case will vary over ~ 20 % of the current wavelength. Thus a relative smoothing length of 30 % should be effective at smoothing away most line features in the smoothed spectrum, but not smoothing the continuum shape too much.

To calculate the large-scale smoothed spectrum itself, a common approach is to simply numerically integrate (e.g., using the trapezoid rule) the spectrum over the box-car interval centered on the current wavelength and divide by the box-car interval to obtain an average flux for the box-car interval which one assigns to the current wavelength. For ordinary small-scale smoothing, nothing special needs to be done about the ends of the spectrum even though they can be treated somewhat wrongly. As an end is approached, the box-car interval gets progressively truncated at that end and the calculated average flux is progressively a less good approximation for the smoothed flux at the current wavelength: it is the smoothed flux for some point in the box-car interval farther from the end. In small-scale smoothing, the smoothing length is comparatively short and somewhat bad behavior at the spectrum ends is usually unimportant. But with a large smoothing length, such as we require for local normalization, this bad behavior at the ends can significantly degrade local normalization near the ends. If the spectrum continuum is relatively flat near the ends, there may be no noticeable degradation. But if the continuum is rising/falling at an end, then the smoothed spectrum becomes too small/large at that end and the locally-normalized spectrum continuum can appear to be rising/falling from 1 at the end. To avoid this problem, we fit a line using least-squares to the spectrum in the box-car interval and determine the smoothed spectrum at the current wavelength from this fitted line. (Actually we fit a line to logarithmic flux as a function of logarithmic wavelength. This means we are fitting the flux to a power-law function of wavelength. See below.) In the interior of the spectrum, this least-squares line fitting gives almost the same result as calculating an average flux for the box-car interval, but at the spectrum ends it usually prevents the locally-normalized continuum from departing obviously from 1. Since spectra are not necessarily very linear (or like a power-law function) over the box-car interval, it is not immediately obvious that this fitting of a line (actually a power-law function in our calculations) should always work well. But the resulting locally-normalized spectra seem generally pleasing to the eye including at the ends and we accept the eye's judgment for our prescription.

In plotting spectra, we often prefer to plot logarithmic flux versus logarithmic wave-

length. The choice of logarithmic wavelength owes to the fact that line profile widths are determined by large Doppler shifts of line opacity wavelength from the rest-frame line opacity wavelength. For example, say a particular component of the line profiles forms in the ejecta moving at velocity v along the line-of-sight counting velocity as positive in the direction away from the observer. For a given line of rest-frame line-center wavelength $\lambda_{\rm line}$, the component will appear in a spectrum at

$$\lambda = \lambda_{\rm line}\sqrt{\frac{1+v/c}{1-v/c}} \approx \lambda_{\rm line}(1+v/c) \ , \tag{8}$$

where we have used the relativistic Doppler shift formula (e.g., Lawden 1975, p. 78; Mihalas 1978, p. 495) and the 1st order (in v/c) Doppler shift formula. (The 1st order Doppler shift formula is usually adequate for supernovae.) From equation (8), we see for a set of lines that the components in a spectrum plot against wavelength will appear at different wavelength shifts from the line-center wavelengths. Thus, the line profiles will tend to have varying widths that scale with $\lambda_{\rm line}$. In spectrum figures, this has an unpleasing effect of making the blue side of a spectrum look relatively crowded with line features and the red side look relatively uncrowded with line features. If one plots using logarithmic wavelength, then the aforementioned particular component is found at

$$\begin{aligned} \log(\lambda) &= \log\left(\lambda_{\rm line}\sqrt{\frac{1+v/c}{1-v/c}}\right) = \log(\lambda_{\rm line}) + \log\left(\sqrt{\frac{1+v/c}{1-v/c}}\right) \\ &\approx \log[\lambda_{\rm line}(1+v/c)] = \log(\lambda_{\rm line}) + \log(1+v/c) \approx \log(\lambda_{\rm line}) + \left(\frac{v}{c}\right)\log(e) \ , \end{aligned} \tag{9}$$

where we have made an expansion of the logarithm to 1st order in v/c which is consistent in order of expansion with the 1st order Doppler shift formula. We see that in logarithmic wavelength, the shift of the particular component is the same for all line profiles (from relativistic Doppler shift formula) and that this shift is approximately proportional to v/c. Thus, the line profiles will tend to have the same width across the spectrum when plotted using logarithmic wavelength. Varying line strength and line blending, of course, prevent the profiles from having an identical appearance when plotted versus logarithmic wavelength. Using logarithmic wavelength gives the plotted spectrum a balanced and pleasing appearance. The above argument for plotting spectra versus logarithmic wavelength applies for both ordinary spectra and locally-normalized spectra.

In plotting ordinary spectra (i.e., not locally-normalized spectra), we often make the choice of plotting logarithmic flux since it gives a more equal appearance to small and large features of a spectrum. Say we take equation (2) (see § 2.1) for the intrinsic flux (which for the sake of argument we assume that we know) and take the logarithm: we get

$$\log\left(f_{\lambda,\rm int}\right) = \log\left(f_{\lambda,\rm con}\right) + \log\left(f_{\lambda,\rm lin}\right) \ . \tag{10}$$

From equation (10), we see that line profiles of the same relative size (i.e., the same $f_{\lambda,\mathrm{lin}}$ profile) will have the same absolute size when logarithmic flux is plotted since the line profiles are just added to the continuum for logarithmic flux and not multiplied by the continuum as in the non-logarithmic case. Of course, varying relative line profile size and line blending will make the logarithmic line profiles vary in absolute size. Nevertheless there is some equalization in line profile appearance in using logarithmic flux. Why do we prefer the more equal appearance of plotting logarithmic flux when large line features, of course, represent larger effects? The reason is that small line features present fine tests for spectrum modeling and clues about quantities (e.g., composition) that may not be apparent in the large line features. Thus, giving more equal weighting to large and small line features makes sense.

Using local normalization has a similar effect to using logarithmic flux: there is an equalization in plotted size of line profiles of the same size relative to the continuum in the ordinary spectra. Nevertheless, we plot the logarithmic flux of the locally normalized spectra in plotting. This is for consistency with our usual practice with ordinary spectra. As mentioned above, in making locally-normalized spectra, we actually use logarithmic flux and logarithmic wavelength in creating fitted lines for the large-scale smoothing rather than just using flux and wavelength. This procedure in creating the locally-normalized spectra tends to make the locally-normalized continuum more like 1 everywhere to the eye on a log-log plot. Locally-normalized spectra calculated using a line fitted to flux as a function of wavelength (which we will call the unlogged locally-normalized spectra) look similar to those calculated with our logarithmic fitting procedure, but the difference is clearly significant to the eye.

Before applying the large-scale smoothing in our local normalization procedure, we also apply to all our spectra a small-scale box-car smoothing (using trapezoid rule integration) with a relative smoothing length of $\delta\lambda/\lambda = 1/300$ which corresponds to a Doppler shift velocity of about $1000\,\mathrm{km\,s^{-1}}$. This smoothing reduces the noise in some of the spectra particularly at the spectrum ends. For some particularly noisy spectra, we sometimes use a larger small-scale smoothing length. The small-scale smoothing should not degrade the spectrum features very much. Supernova line features generally vary relatively slowly over wavelength scales corresponding to Doppler shift velocities of order $1000\,\mathrm{km\,s^{-1}}$. Interstellar and telluric lines can vary rapidly on shorter wavelength scales, but these are not intrinsic to supernova spectra and could be eliminated from the spectra if necessary.

A stand-alone fortran-95 code locnorm.f for making locally normalizing spectra is available for downloading from SUSPEND under the heading *Useful Programs*. All the supernova spectra currently in SUSPEND are shown plotted in original and locally-normalized format under the heading *Supernovae by Epoch* in html files in supernova directories.

3. EXAMPLES OF LOCALLY-NORMALIZED SUPERNOVA SPECTRA

Figures 1, 2, 3, and 4 (which we discuss individually below in separate subsections) show locally-normalized supernova spectra plotted on log-log plots together with the original spectra in the wavelength representation (i.e., f_λ or flux-per-unit-wavelength representation): the locally-normalized spectra are obviously the ones with continuum levels of about 1 and the original spectra have been vertically shifted to be well displayed. The spectra are all for Type IIb supernova SN 1993J which occurred in M81 (NGC 3031). They have been dereddshifted using host galaxy heliocentric velocity $-39 \pm 2\,\mathrm{km\,s^{-1}}$ from Leda (Paturel et al. 2003). (Since the host galaxy heliocentric velocity is negative, the spectra are, of course, actually redshifted to be put in the rest frame.) The original spectra have not been dereddened. The $E(B-V)$ reddening value for SN 1993J is quite uncertain. Richmond et al. (1994) after a lengthy consideration of many methods of determining $E(B-V)$ for SN 1993J suggest that the SN 1993J $E(B-V)$ value is in the range ~ 0.08–$0.32\,\mathrm{mag}$ which is a range from low to moderate $E(B-V)$. The possible intrinsic spectra obtained by correcting an observed spectrum using $E(B-V)$ values from this range and a standard reddening law (e.g., Cardelli et al. 1989; O'Donnell 1994) would show a considerable range in continuum behavior. Thus, the intrinsic continuum behavior of SN 1993J for any phase is quite uncertain. Avoiding the uncertainty in dereddening and calibrating observed spectra is one of the main reasons for using local normalization as discussed in § 1.

Because M81 is at a distance of only $3.63 \pm 0.34\,\mathrm{Mpc}$ (as determined from Cepheids (Freedman et al. 1994)), SN 1993J became a very bright and well-observed supernova. It was discovered on 1993 March 28.86 UT (JD 2449075.36) (Ripero 1993) which was probably only about a day after explosion (or core collapse) which may have been 1993 March 27.9 ± 0.2 (JD 2449074.4 ± 0.2) (Richmond et al. 1994). An initial very high peak in UVOIR bolometric brightness was partially observed (e.g., Richmond et al. 1994): this peak, which probably happens for all core-collapse supernovae soon after shock break-out, is usually unobserved, and so is not used to define conventional UVOIR bolometric maximum light even though it may often/always be higher than conventional UVOIR bolometric maximum light as it is for SN 1993J. SN 1993J's (conventional) maximum lights occurred on 1993 April 16 (JD 2449093.7) in B, 1993 April 17 (JD 2449095.0) in V, and 1993 April 17 ± 1 (JD 2449094.7 ± 1.0) in UVOIR bolometric luminosity (Richmond et al. 1994). The UVOIR bolometric luminosity rise time to maximum light was about 20 days (Richmond et al. 1994). The maximum B and V apparent magnitudes were, respectively, 11.35 ± 0.05 and 10.80 ± 0.05 (Richmond et al. 1994).

SN 1993J was originally classified as a Type II supernova because it had conspicuous hydrogen Balmer lines. However, these lines did not become as strong as in typical Type II

supernovae and by about 40 days after explosion SN 1993J evolved to resemble Type Ib supernovae (e.g., Filippenko & Matheson 1993). Type Ib supernovae have metal lines and conspicuous helium lines and, it seems in general, hydrogen lines that are somewhat weak and hard to identify especially after maximum light (Branch et al. 2002). Supernovae that undergo a transformation from Type II to Type Ib have come to be called Type IIb's using a term invented by Woosley et al. (1987) in a theoretical prediction that small-hydrogen-envelope supernovae could exist. Type IIb's are considered to be hydrogen-deficient compared to ordinary Type II supernovae, but probably have more hydrogen than Type Ib/c's. The observational prototype Type IIb is SN 1987K (Filippenko 1988). Two other Type IIb supernovae with a significant number of published spectra are SN 1996cb (Qiu et al. 1999; Matheson et al. 2001) and SN 1998fa (Matheson et al. 2001). As of 2007 March 8, the supernova list of Central Bureau for Astronomical Telegrams (2007) contains 25 Type IIb or possible Type IIb supernovae (including SN 1987K which is actually listed as a Type II).

The ejecta of SN 1993J had a shock interaction with a thick circumstellar wind shed by the supernova progenitor as evidenced by radio and X-ray emission (e.g., Fransson et al. 1996, and references therein). In this respect, SN 1993J was like the Type II supernovae SN 1979C and SN 1980K which also showed strong radio emission (e.g., Weiler et al. 1986). The interaction also had an effect on the UV spectra of SN 1993J similar to that on SN 1979C and SN 1980K. We will discuss this UV effect briefly in § 3.2.

We have made some line identifications in the figures by labels giving the line's parent ion or specific line name in the case of the Balmer lines. The labels are only given for the lines in the locally normalized spectra since the corresponding lines in the original spectra are identified by comparison to the locally normalized spectra. For clear P Cygni lines, we put the identification labels with the blueshifted absorption features of the P Cygni lines since this is usually the most distinct part of the line profiles. For emission lines, we put the identification labels with the emission features of the emission lines. P Cygni lines dominate optical/IR spectra in the photospheric phase and emission lines in the nebular phase. Figures 1 and 2 show photospheric phase spectra and Figures 3 and 4 show nebular phase spectra.

We should remark that in the photospheric phase, a supernova is optically thick in the optical/IR. As the supernova expands, the opacities must fall with decreasing density and the supernova gradually enters the nebular phase where the supernova is optically thin in the optical/IR. Supernovae tend to remain optically thick in the UV for much longer than in the optical/IR because there are many strong metal lines in the UV particularly from the iron-peak elements. There is no sharp dividing time between the two phases. One often just starts using the term nebular phase when the emission features start to dominate the optical/IR

line pattern. There is also no sharp distinction between P Cygni lines (possessing blueshifted absorptions and emission features usually centered on the rest-frame line-center wavelengths) and emission lines (which are just emission features usually centered on the rest-frame line-center wavelengths). (The centering of emissions on the rest-frame line-wavelengths is often approximate and sometimes the emissions are significantly shifted. For example, strongly blueshifted emission lines can occur in the UV. For examples of such emission lines, see §§ 3.2–3.4.) In practice, when the absorption feature of a P Cygni line has become hard to identify, we can say it has become or nearly become an emission line.

We should also remark that supernova matter after the explosion phase is in uniform motion and the whole ejecta structure just scales up linearly with time t since the explosion which is effectively a point event. This motion is called homologous expansion. In homologous expansion, the radial velocity of any matter element of ejecta is a good comoving-frame radial coordinate and we use it as such as is customary in supernova studies. The densities of the matter elements in the ejecta scale as t^{-3}.

3.1. Figure 1: the 1993 March 31 Spectrum

Because of its closeness and brightness, SN 1993J was spectroscopically very well observed with the earliest spectrum taken on 1993 March 29.88 UT (JD 2449076.38) with the Isaac Newton Telescope by E. Perez and D. Jones (Clocchiatti et al. 1995). The spectrum in Figure 1 is also an early one from 1993 March 31 (JD 2449078.35) (Barbon et al. 1995) which is about 4 days after explosion and is about 16 days before UVOIR bolometric maximum light. The original spectrum rises very steeply to the blue showing that the supernova photosphere was very hot at this phase. From Figure 11 of Richmond et al. (1994), we estimate that a blackbody spectrum fit to the spectrum (if it was well calibrated) for this phase would give a blackbody temperature in the range $\sim$ 12000–23000 K where the range is caused by the uncertainty in the reddening. The uncertainty in spectrum temperature highlights the difficulty in relying on continuum shape for determining the physical properties of supernovae from heterogeneous types with uncertain reddening and supports our argument for giving more weight to the line pattern than to the continuum shape (see § 1).

We have identified the lines in Figure 1 mostly following Barbon et al. (1995) and Baron et al. (1995). For this spectrum and the others below, we also rely on our general understanding of spectrum formation in making identifications. The Hδ identification is uncertain because the absorption feature identified as possibly due to Hδ is rather weak and indefinite. The He I line is He I λ5875.7 (e.g., Wiese et al. 1966, p. 14) and the Ca II line actually arises from the Ca II IR triplet (i.e., Ca II λ8579.1, where we have cited the

gf-weighted mean line wavelength: the component lines are at 8498.02 Å, 8542.09 Å, and 8662.14 Å) (e.g., Wiese et al. 1969, p. 251). (Hereafter we usually cite only the gf-weighted mean line wavelength for multiplets.) The line velocities (i.e., the velocities corresponding to the Doppler blueshifts of the line absorption minima from the rest-frame line-center wavelengths) are about 11000 km s^{-1} (Hδ if this is the correct identification), 5900 km s^{-1} (Hγ), 13400 km s^{-1} (Hβ), 12800 km s^{-1} (He I), 12700 km s^{-1} (Hα), and 26800 km s^{-1} (Ca II IR triplet). We use the gf-weighted mean wavelengths for calculating the line velocities of multiplets. (Here and throughout our discussion, wavelength measurements are made from the locally-normalized spectra and we do a little smoothing by eye to determine the minima when needed.) The low velocity of Hγ may be because of line blending with Hδ since the lines are separated in Doppler shift velocity by only 17000 km s^{-1}. The much higher velocity for the Ca II IR triplet line than for the other lines makes the identification a bit uncertain, but there seems nothing else it could be. In fact, high-velocity line features, for lines including the Ca II lines, have been found for at least one other HDCC supernova (Type Ibc SN 2005bf (Folatelli et al. 2006; Parrent et al. 2007); see § 1 for HDCC supernovae) and the work of Parrent et al. (2007) imples that high-velocity line features might be common in Type Ic supernova spectra. (By high-velocity features, we mean line absorptions forming well above the photosphere at velocities of perhaps $\gtrsim$ 15000 km s^{-1}.) Given the above remarks, it is possible, speaking speculatively, that HDCC supernovae of all kinds (such as Type IIb SN 1993J) might have some high-velocity line features in some cases.

A remarkable feature of the line pattern is that the Hβ line is much stronger than the Hα line: this cannot happen in local-thermodynamic equilibrium (LTE). The feature may require a non-LTE (NLTE) explanation. On the other hand, the feature may be a result of an observational error of some kind since another SN 1993J spectrum from the same day reported by Baron et al. (1995) does not clearly show the Hβ line stronger than the Hα line. In any case, Baron et al. (1995) using the NLTE code PHOENIX were able to fit the continuum well, but not the lines for the March 30–31 phase of SN 1993J. Their difficulty may lie in the inaccurate physical structure of their model and/or an inaccurate reddening correction.

3.2. Figure 2: the 1993 April 15 Spectrum

Figure 2 shows the SN 1993J spectrum from 1993 April 15 (Jeffery et al. 1994): this was 2 days before UVOIR bolometric maximum light and about 18 days after explosion. The spectrum is a combination of an *HST* UV-blue-optical spectrum and Lick Observatory ground-based spectrum. The *HST* spectrum was obtained as part of the *HST* Supernova

INtensive Study (SINS) General Observer program (Kirshner et al. 1988). The two spectra agreed well in shape and scale in their overlap region 3120–3276 Å, and so we simply joined them at 3240 Å cutting off the overlapping ends. The line identifications mostly follow from Jeffery et al. (1994) and Baron et al. (1995). The line velocities are in the range $\sim$ 7000–11000 km s^{-1} (Jeffery et al. 1994). We emphasize though that the lines are often blended and the identifications in many cases only indicate the strongest contributor to the line feature. The 4 strongest hydrogen Balmer lines, the He I λ5875.7 line and the Ca II IR triplet line are again present. We note that Hα is now the strongest line in the optical part of the spectrum (but note that the Mg II line in the UV is comparably strong: see below) and that it is in net emission which is typical of Hα lines in Type II supernovae.

The absorption centered at about 3835 Å is caused by the Ca II H&K lines: i.e., the multiplet Ca II λ3945.2 (e.g., Wiese et al. 1969, p. 252). This multiplet is very strong because it is a resonance multiplet (i.e., it arises from the ground level). The line velocity for the Ca II H&K lines is 8360 km s^{-1}. The Fe II lines mainly arise from the multiplets Fe II λ4555, Fe II λ4561, and Fe II λ5060 (e.g., Kirshner et al. 1993, Table 4). The absorption centered at about 7570 Å may be the absorption of a P Cygni line caused by the multiplet O I λ7773.4 (e.g., Wiese et al. 1966, p. 79). This line is common in Type Ib/c supernovae (e.g., Branch et al. 2002) and Type Ia supernovae (e.g., Kirshner et al. 1993), but unfortunately its absorption usually coincides with a strong telluric line and it is sometimes, as here, unclear if the telluric line has been adequately corrected for. We regard this identification as tentative. If the identification is correct, the O I λ7773.4 line velocity is 7830 km s^{-1}. By about 40 days past UVOIR bolometric maximum light, the O I λ7773.4 line seems clearly present (Barbon et al. 1995).

The UV of SN 1993J is similar to that of SN 1979C and SN 1980K and is probably greatly modified from what a bare supernova would have given by circumstellar shock interaction (Jeffery et al. 1994). In a series of papers, Fransson (1982, 1984a,b) and Fransson et al. (1984c) have given a detailed model of supernova UV behavior with circumstellar interaction: this work was stimulated by International Ultraviolet Explorer (*IUE*) data for SN 1979C and SN 1980K. In brief, some fraction of UVOIR light from the supernova photosphere is scattered by shock-heated electrons in the shock region of ejecta and circumstellar matter and Comptonized (i.e., blueshifted up to the UV or extreme UV). Also there will be X-ray emission from the shock-heated gas. Some of the Comptonized light and X-ray emission just escapes the supernova environment, but some back-heats the outer supernova ejecta and creates a complex, layered, photoionization region in the outer supernova atmosphere. The emission from back-heating adds to the direct emission from the supernova interior that emerges at the photosphere. In the optical, this emission from back-heating is probably negligible (except in some lines), but in UV blueward of perhaps $\sim$ 2800 Å it appears to

become important by comparison to spectra from supernovae with little or no circumstellar interaction (Jeffery et al. 1994). As well as continuum emission from recombination and free-free emission, UV emission lines from ionized atoms can make a considerable contribution: the prominent UV emission lines are primarily resonance lines that have been collisionally excited by the back-heated medium. The layers of Comptonized-flux photonization form a geometrically narrow shell of ejecta moving at velocities of order $10^4\,\mathrm{km\,s^{-1}}$. The observer sees the emission from back-heating primarily from this shell. Below the shell is the optically thick photosphere. Thus, the observer mostly sees the emission from back-heating from the near-side of the ejecta with line-of-sight velocities ranging from much less than $10^4\,\mathrm{km\,s^{-1}}$ away from the observer up to line-of-sight velocities of order $10^4\,\mathrm{km\,s^{-1}}$ toward the observer. For UV emission lines, the varying Doppler shift given by the moving shell will result in broad blueshifted emission features.

An effect that tends to enhance blueshifted line emission from a shell surrounding an opaque photosphere is diffuse reflection toward the observer of the line emission from the photosphere (Chugai 1988). This reflected line emission must mainly come from the near side of the photosphere, and thus will tend to be mainly blueshifted from the rest-frame line-center wavelength and hence the enhancement of the blueshifted line emission. If the interior of the shell were transparent, the light that could otherwise be reflected would simply stream away from the observer and all redshifted line emission from the far side of the shell would come toward the observer. The reflection can be caused by scattering from electrons, but in the UV, particularly in the nebular phase when the electron optical depth through the ejecta has become small, the reflection is probably mainly by scattering from the many iron-peak-element lines in the UV. To understand the reflection effect clearly, imagine an ideal case of a perfectly reflecting photosphere just interior to a very geometrically thin line-emitting shell. Virtually all the line emission from the near side of the shell moving inward would be reflected from the near side of the photosphere and some would go to the observer. Virtually no emission or reflection would come to the observer from, respectively, the far side of the shell or the far side of the photosphere. Since the photosphere matter is expanding homologously, the reflected light toward the observer will be mostly blueshifted. Note that in moving inward toward the photosphere, the line emitted photons will redshift from the rest-frame line-center wavelength in the comoving frame and that the photosphere is moving a little more slowly than the shell. (Propagating photons always redshift in the comoving frame in homologously expanding atmospheres no matter what the degree of special relativistic effects (Jeffery 1993).) Consequently, the light reflected toward the observer will tend on average to be less blueshifted in the observer frame than the line emission coming directly from the line-emitting shell. Because the photosphere is just interior to the shell in our ideal case, this redshift effect will be small. In a real case, the shell will not necessarily be

very geometrically thin, and so some significant amount of redshifted flux from the far side of the line-emitting shell could reach the observer. Also some fraction of the observer-directed reflected light (mainly from near the photosphere limb where the line-of-sight velocity of the photosphere is small) will end up a bit redshifted from the line-center wavelength in the observer frame because of the redshift in the comoving frame that happens while the light moves inward toward the photosphere. But the contribution of this redshifted reflected light is probably relatively small in most cases. Note also, a real photosphere will not, of course, be perfectly reflecting: some of the line emission will be absorbed and its energy dispersed to other parts of the spectrum.

We have not attempted a full identification of features seen in the UV region of the spectra we present. However, the strong emission-like feature peaking at 2717 Å in the spectrum must be the resonance multiplet Mg II λ2797.9 (e.g., Wiese et al. 1969, p. 30; Moore & Merrill 1968, p. 10) blueshifted and in emission and produced as discussed by Fransson. (The emission features most fully analyzed by Fransson were primarily those from blueward of 2000 Å, but his analysis seems to apply to Mg II λ2797.9 as well.) In SN 1979C UV *IUE* spectra (INES 2000), a similar blueshifted Mg II λ2797.9 emission appeared possibly about 7 days after optical maximum light (1979 April 22) (Panagia et al. 1980), became definite by 33 days past optical maximum (1979 May 18), and was still clearly present in the last *IUE* observation about 111 days past maximum (1979 August 4). (Optical maximum light for SN 1979C was about 1979 April 15 (Barbon et al. 1982).) In SN 1980K UV *IUE* spectra (INES 2000), a similar blueshifted Mg II λ2797.9 emission seems to have arisen about 26 days after optical maximum light (1980 October 30) and be present on the last *IUE* observation from about 62 days past optical maximum (1981 January 5). In the SN 1980K spectra, the emission is generally less clear than in SN 1979 spectra, but it definitely present about 35 days past optical maximum (1980 December 9). (Optical maximum light of SN 1980K was about 1980 November 4 (Buta 1982).) We note that an Mg II λ2797.9 emission line is a common feature of quasar emission-line clouds (e.g., Reichard et al. 2003) which may somewhat resemble the UV emission shell of circumstellar-interacting supernovae (Fransson 1984b).

The Mg II λ2797.9 emission peak wavelength 2717 Å corresponds to a Doppler blueshift velocity of 8700 $\mathrm{km\,s^{-1}}$ which is within the range of P-Cygni line velocities in the optical $\sim$ 7000–11000 $\mathrm{km\,s^{-1}}$ (Jeffery et al. 1994). If we just define 2700 Å as the characteristic blue edge of the Mg II λ2797.9 emission (which is good for later phases: see §§ 3.3 and 3.4 below), the corresponding Doppler blueshift velocity is 10500 $\mathrm{km\,s^{-1}}$. We take this velocity as the characteristic velocity of the Mg II λ2797.9 emission shell.

Without strong circumstellar interaction, the Mg II λ2797.9 multiplet would probably

contribute along with Fe II lines to a blueshifted P-Cygni absorption feature. For Type Ia supernovae, the absorption can be seen in the *HST* spectra of SN 1992A in the photospheric phase (Kirshner et al. 1993) and, perhaps, well into the nebular phase at 291 days after B maximum light although not so identified (Ruiz-Lapuente et al. 1995). For Type II supernovae, the absorption can be seen in the *IUE* spectra of SN 1987A (Pun et al. 1995). The difference for the Mg II λ2797.9 multiplet between having blueshifted emission and having blueshifted absorption is probably explained by saying that with circumstellar interaction the line-forming region is hotter than the inner ejecta and without circumstellar interaction it is colder.

No other identifications in the UV of SN 1993J are probably possible without a more detailed analysis. We leave that to future work *sine die*.

3.3. Figure 3: the 1993 September 15.5 Spectrum

Figure 3 shows the SN 1993J spectrum that we have constructed from a 1993 September 17 *HST* UV-blue-optical spectrum and a 1993 September 14 ground-based spectrum taken at the MMT Observatory by P. Challis and C. S. J. Pun. We will call the combined spectrum the 1993 September 15.5 spectrum: thus it comes from about 151 days after UVOIR bolometric maximum light and 171 days after explosion. Both component spectra were obtained as part of the SINS program and neither have been published before (Challis 2006, for the *HST* spectrum; Blondin 2007, for the MMT spectrum). The *HST* spectrum has not been given a definitive flux calibration (Challis 1994). The two spectra agreed well in shape in the region 4250–4781 Å, and so we simply and joined them at 4253.6 Å cutting off the overlapping ends. The ground-based spectrum had to be scaled by a factor of 0.35.

The supernova at the time of this spectrum is clearly in the nebular phase because of the strong optical/near-IR emission lines. The line identifications for the 3 strongest emission lines in the optical/near-IR are based on analysis of Houck & Fransson (1996) for a 1993 August 15 SN 1993J spectrum: the extrapolation of the identifications to 1993 September 15.5 is reliable because these lines are strong, persistent, and well identified in other HDCC supernovae. The actual lines are the forbidden multiplet [O I] $\lambda\lambda 6300, 6364$ which is a resonance multiplet (e.g., Wiese et al. 1966, p. 82) and the forbidden multiplet [Ca II] $\lambda\lambda 7291, 7324$ (e.g., Wiese et al. 1969, p. 255) and, again, the Ca II IR triplet.

The absorption with minimum at 3829 Å is caused by Ca II H&K lines (the resonance multiplet Ca II λ3945.2). The line velocity of the Ca II H&K lines is $8800\,\mathrm{km\,s^{-1}}$. There is no obvious strong emission feature associated with these lines. Evidently, the Ca II H&K

lines are optically thick and strongly trap photons in the spatial resonance regions of the lines. The trapping process is as follows. As photons are propagating through the supernova atmosphere, they redshift into resonance with the lines in some location (i.e., a resonance region) and are absorbed and then resonantly emitted, but cannot easily redshift out of resonance because of continually being re-absorbed and re-emitted in the lines after traveling and redshifting very little. So there are many re-absorptions and re-emissions. Much of the photon energy ultimately escapes by being emitted by the Ca II IR triplet which shares the same upper level with the Ca II H&K lines (e.g., Moore & Merrill 1968, p. 12): this energy leak mostly suppresses the emission feature of the Ca II H&K lines. The lower level of the Ca II IR triplet is metastable and the upper level of the forbidden multiplet [Ca II] $\lambda\lambda 7291, 7324$ (e.g., Moore & Merrill 1968, p. 12). Collisions are weak in the nebular phase due to low density, and hence the transitions from the metastable lower level of the Ca II IR triplet to the ground level become increasingly radiative which results in the strong [Ca II] $\lambda\lambda 7291, 7324$ emission feature. The process of energy from absorption in the Ca II H&K lines being emitted in other redder lines is an example of fluorescence (e.g., Mihalas 1978, p. 22).

In the UV, the blueshifted Mg II $\lambda 2797.9$ emission line now peaks at 2726 Å which corresponds to Doppler blueshift velocity of $7700\,\mathrm{km\,s^{-1}}$ and has now increased in height to about 3.4 times the continuum level. Its overall shape, however, is much the same as earlier on 1993 April 15 (see Fig. 2 in § 3.2 and Fig. 5 in § 3.4).

The peak centered at 4563 Å may be at least in part the emission feature of the semi-forbidden line Mg I] $\lambda 4571$ (e.g., Moore & Merrill 1968, p. 16; Wiese et al. 1969, p. 26; NIST 2007). The emission is relatively weak, but Houck & Fransson (1996) predict Mg I] $\lambda 4571$ as a weak emission line (seemingly blended with some other emission line) for 1993 August 15 and believe the Mg I] $\lambda 4571$ emission should become stronger with time. If the 4563 Å emission is primarily Mg I] $\lambda 4571$, then the line has been Doppler blueshifted by velocity $\sim 500\,\mathrm{km\,s^{-1}}$. The 1993 November 15.5 spectrum in Figure 4 (see § 3.4) shows a stronger emission peaking at 4551 Å and if this is caused by Mg I] $\lambda 4571$, then it has been Doppler blueshifted by velocity $\sim 1300\,\mathrm{km\,s^{-1}}$. The 1993 November 15.5 spectrum emission peaking at 4551 Å, however, has a secondary peak at almost exactly 4571 Å. This suggests that the main peak is caused by some other line in emission and not Mg I] $\lambda 4571$. In order for the 4563 Å and 4551 Å emissions to be primarily Mg I] $\lambda 4571$, there must be some blueshifting asymmetry in the ejecta or some significant continuum optical depth. (A significant continuum optical depth would tend to suppress the red side of an emission line.) We note that the [O I] $\lambda 6300$ emission peaks at 6302 Å (corresponding to a Doppler redshift velocity of $\sim 100\,\mathrm{km\,s^{-1}}$) in the 1993 September 15.5 spectrum and at 6300 Å (corresponding to virtually no Doppler shift at all) in the 1993 November 15.5 spectrum. The lack of significant shifts in the [O I] $\lambda 6300$

emission peaks argues for symmetric ejecta and optically thin ejecta in the optical. There is the complication, however, that the blue side of the optical generally has more significant weak lines than the red side of the optical and may persist being somewhat optically thick longer than the red side due to a quasi-continuum opacity of the weak lines. The upshot of all these considerations is that we draw no conclusion about the identities of the 4563 Å and 4551 Å emissions. These emissions may be blueshifted Mg I] λ4571 or Mg I] λ4571 blended with some other emission line, but more analysis is needed.

(The case for Mg I] λ4571 identification in the optical is different than for the Mg II λ2797.9 identification in the UV. We expect the nebular-phase ejecta to be optically thin or relatively optically thin in the optical and optically thick in the UV at least for a long time into the nebular phase. The UV optical thickness in the nebular phase is the cause of the blueshift of the Mg II λ2797.9 emission as we argued in § 3.2.)

We note that the strong emission features in the optical/near-IR in both versions of the spectrum, but particularly in the locally-normalized version, seem to be adjacent to absorptions. There may be real strong absorptions at these locations from lines that are optically thick, but a synthetic spectrum analysis is probably needed to show that. The locally-normalized spectra for the nebular phase, however, may be a bit deceptive. The process of local normalization will tend to make emission features sit in troughs that are below 1, and thus create the appearance of adjacent absorptions. In reality, the emission lines may just be added to a fairly smooth continuum that holds across the spectrum (or at least the optical/IR spectrum) and there may be no significant absorptions (at least in the optical/IR spectrum). So in regard to nebular spectra, local normalization as we have implemented it may not be ideal in that it probably cannot scale a real physical nebular continuum to nearly 1 at least in the vicinity of strong emission features. On the other hand, there may be no well-defined physical continuum level in which case applying local normalization does not obviously worsen the appearance of the spectra for analysis. Our arguments for local normalization based on avoiding dealing with uncertain reddening and calibration error (§ 1) are still valid for the nebular phase. Figure 3 and Figure 4 (§ 3.4) do show that local normalization even in the nebular phase will, of course, tend to cause the average flux level to be near 1.

For the photospheric phase, local normalization is probably much better at setting the phyisical continuum to near 1 than for the nebular phase. First, there is a significant real physical continuum in the spectrum (although it is probably almost never a pure blackbody continuum) which is not necessarily the case in the nebular phase. Second, the smoothing of the P Cygni absorptions and emissions to create the large-scale smoothed spectrum is an averaging that must put the large-scale smoothed spectrum close to the physical continuum

level. The locally-normalized spectrum will then have a continuum close to 1.

3.4. Figure 4: the 1993 November 15.5 Spectrum

Figure 4 shows the SN 1993J spectrum that we have constructed from a 1993 November 14 *HST* UV-blue-optical spectrum and a 1993 November 17 Lick Observatory ground-based spectrum both of which were obtained as part of the SINS program. The *HST* spectrum has not been published before (Challis 2006); the Lick spectrum was taken by A.V. Filippenko and T. Matheson (Filippenko 1994). We will call the combined spectrum the 1993 November 15.5 spectrum: thus it comes from about 212 days after UVOIR bolometric maximum light and 232 days after explosion. The *HST* spectrum has not been given a definitive flux calibration (Challis 1994) and the ground-based spectrum is not absolutely calibrated, although its relative calibration is excellent (Filippenko 1994). The two spectra agree well in shape in the overlap region 3120–4781 Å, and so we simply joined them at 4200 Å cutting off the overlapping ends. The ground-based spectrum, after converting it from the frequency representation to the wavelength representation, had to be scaled by a factor of 5.55×10^{-9} to account for overall calibration differences and for unit transformation. The *HST* spectrum blueward of ~ 2425 Å seems to decline in a manner too steep to be physically real and we do not trust it (nor the locally-normalized spectrum we derive from it) there.

Qualitatively, the 1993 November 15.5 spectrum is much like the 1993 September 15.5 spectrum. (We are relying on the locally-normalized spectra for comparisons.) The Mg II λ2797.9, [O I] $\lambda\lambda 6300, 6364$, and [Ca II] $\lambda\lambda 7291, 7324$ emissions have increased in height relative to the continuum and the Ca II IR triplet emission has decreased. The peak of the Mg II λ2797.9 emission is at 2726 Å just as in the 1993 September 15.5 spectrum. The emission at peaking at 4563 Å (whatever it may be) in the 1993 September 15.5 spectrum has increased and shifted so that it now peaks at 4551 Å. (See the discussion of this emission feature in § 3.3.) The Ca II H&K absorption is not as deep as in the 1993 September 15.5 spectrum.

In Figure 5, we show the time development of Mg II λ2797.9 emission in locally-normalized spectra. Although the emission line scales up with time, its appearance is remarkably stable. Our definition of 2700 Å as the characteristic blue edge of the Mg II λ2797.9 emission (with corresponding Doppler blueshift velocity $10500\,\mathrm{km\,s^{-1}}$; see § 3.2) is valid for all the phases we display. The behavior of the spectra in the region $\sim$ 2780–2820 Å is not very certain since we have just omitted wavelength points that correspond to the interstellar Mg II λ2797.9 lines which arise from gas clouds along the line of sight to the supernova. Such clouds, identified from interstellar lines of various ions, have heliocentric

velocities in the range from about -140 to 181 $\mathrm{km\,s^{-1}}$ (Wamsteker et al. 1993; Wheeler et al. 1993).

Later *HST* UV spectra of SN 1993J from day +649 to about day +2561 relative UVOIR bolometric maximum light show the Mg II λ2797.9 emission as box-like in appearance and more symmetrical about the rest-frame line-center wavelength than in the spectra we show (Fransson et al. 2005). The Mg II λ2797.9 emission in the later spectra have a Doppler velocity full-width of $\sim$ 17000 $\mathrm{km\,s^{-1}}$. It seems that the circumstellar interaction back-heating persists through the later phases, but the optical depth through the ejecta has greatly diminished, and thus occultation of the far side of the Mg II λ2797.9 shell has greatly decreased. The flattish top of the late Mg II λ2797.9 emission line is characteristic of emission lines from expanding, optically thin shells as first shown by Beals (1931): other references for the flat-top emission from expanding shells are Mihalas (1978, p. 477) and Jeffery & Branch (1990, p. 190).

3.5. The Continuum Independence of Local Normalization

The main goal of local normalization is to eliminate variations in the continuum in comparing spectra. Implicit in this goal is the requirement that locally-normalized spectra be virtually independent of the continuum shape. For example, if this were not the case, intrinsic spectra that were identical, but with observed continuums distorted in various ways, could be transformed to different locally-normalized spectra and one would reach the false conclusion that the intrinsic spectra were not identical. To test local normalization for continuum independence, we have weighted each of the four original spectra in this section by λ^2 (effectively converting the spectra to the f_ν representation) and λ^4 and then locally normalized these weighted spectra and compared them to each other and the unweighted locally-normalized spectra.

For each original spectrum, a plot (using an expanded scale compared to that spectrum's plot in Fig. 1–4) of the corresponding locally-normalized spectra calculated with and without weights shows exact overlap to the eye of the locally-normalized spectra. On the other hand, the unlogged locally-normalized spectrum (see § 2.2) corresponding to an original spectrum was distinct from the other locally-normalized spectra for that original spectrum when plotted: the unlogged locally-normalized spectrum was generally a bit lower than the other locally-normalized spectra.

As mentioned in the Introduction (§ 1), DIFF1 is essentially a mean relative difference between the line patterns of two spectra, and thus the reader can roughly understand DIFF1

values before seeing the precise formula (which is given below in § 4.1). The DIFF1 values for spectrum pairs consisting of the locally-normalized weighted spectra and the locally-normalized unweighted spectra (all derived from the same original spectrum) were of order 0.001–0.0015 for weight λ^2 and of order 0.002–0.003 for weight λ^4. These are very small mean relative differences. On the other hand, DIFF1 tests of the unlogged locally-normalized spectra with the corresponding other locally-normalized spectra gave DIFF1 values of order 0.4–0.7 which are comparable to DIFF1 values between locally-normalized spectra of the same supernova from phases differing by several days.

We conclude that local normalization will transform continuum-distorted versions of an original spectrum to virtually the same locally-normalized spectrum. Thus, local normalization is sufficiently continuum-independent to lead to valid results in comparing locally normalized spectra. On the other hand, different local normalization procedures can produce noticeably distinct locally-normalized spectra for a given original spectrum. Thus, one should choose a single local normalization procedure and stick with it for valid comparisons of locally-normalized spectra.

4. DIFF1 AND DIFF2

In this section, we introduce the formulae for DIFF1 (§ 4.1) and DIFF2 (§ 4.2), show an example of two locally-normalized spectra fitted by minimizing the DIFF2 function value (§ 4.3), and compare DIFF1 and DIFF2 (§ 4.4).

4.1. DIFF1

Say f_i is the locally-normalized flux at wavelength λ_i. Let

$$\delta_i = f_i - 1 \tag{11}$$

be the flux difference at wavelength λ_i. The flux difference is the relative difference of the line pattern from the continuum for the original spectrum or the absolute difference of the line pattern for the locally-normalized spectrum. We define DIFF1 between a spectrum 1 and a spectrum 2 by the formula

$$\mathrm{DIFF1} = \frac{1}{I} \sum_i \frac{|\delta_{1,i} - \delta_{2,i}|}{\max\left(|\delta_{1,i}|, |\delta_{2,i}|, \xi\right)} \ , \tag{12}$$

where the subscripts 1 and 2 indicate the spectrum and I is the total number of wavelength points in the summation. (The wavelength points are equally spaced in logarithmic wave-

length: see below.) The ξ is a small number that we set to 10^{-15}. This is typically the smallest number that added to 1 that creates a number significantly different from 1 with fortran 95 double precision arithmetic. The ξ prevents arithmetic exceptions, but is only very rarely invoked.

From equation (12), it is clear why we describe DIFF1 as the mean relative difference in line pattern between two spectra (see §§ 1 and 3.5). If DIFF1 $<<$ 1, the spectra will be much alike. If DIFF1 $\gtrsim$ 1, the spectra will be substantially different. For example, if the flux differences (i.e., the δ_i's) for one spectrum in a DIFF1 test were almost all only a small fraction of those for the other spectrum (i.e., one spectrum had much weaker lines than the other), the DIFF1 value would be close to 1. In fact, the DIFF1 function has an upper limit:

$$|\delta_{1,i} - \delta_{2,i}| \leq |\delta_{1,i}| + |\delta_{2,i}| \leq 2\max\left(|\delta_{1,i}|, |\delta_{2,i}|\right) \leq 2\max\left(|\delta_{1,i}|, |\delta_{2,i}|, \xi\right) \ , \tag{13}$$

and thus

$$\mathrm{DIFF1} \leq 2 \ . \tag{14}$$

We would not usually expect a DIFF1 value approaching 2 since that would mean that two input locally-normalized spectra had line patterns that were nearly mirror images of each other about the continuum level: i.e., the line patterns would be strongly anticorrelated. In fact, any DIFF1 values well over 1 would show some anticorrelation between spectrum line patterns. There is no strong physical reason to expect much anticorrelation of supernova spectrum line patterns, but some accidental anticorrelation should happen, and so some DIFF1 values over well over 1 may occur when applying DIFF1 to heterogeneous samples of spectra.

We have subjected the set of all possible spectrum pairs drawn from the sample of HDCC supernovae described in § 5 to the DIFF1 test. (There are 17 supernovae, 168 spectra, and 27588 valid spectrum pair tests: some possible pair tests are excluded as invalid by the validity criterion discussed below.) The resulting distribution of DIFF1 values has mean, standard deviation, minimum value, and maximum value of, respectively, 0.865, 0.137, 0.244, and 1.320 (where we have reported more digits than are significant to allow for numerical consistency checks). That the mean 0.865 is so close to 1 (actually within 1σ of 1) shows that spectrum pairs on average are not highly similar. This is understandable since the spectra come from a heterogeneous sample of supernovae and from many phases: the spectrum of a supernova can evolve significantly with phase. The standard deviation value shows that spectrum pairs significantly (i.e., 1σ) more alike than average will have DIFF1 values of $\lesssim 0.73$. The minimum 0.244 suggests that even spectra from the same supernova at close to the same phase vary from each other significantly. Note we have excluded redundant spectra from the same phase period (which we usually set to being 1 day) for a supernova

(as described in § 5.1) since those should be nearly identical to the included spectrum aside from observational error. As we expected, the maximum DIFF1 value is much less than 2.

We note that if we used f_i's in the formula for DIFF1 (i.e., eq. (12)) instead of δ_i's (which would only change denominators, in fact), we would have lessened the sensitivity to line patterns. For example, Type IIb and Type Ic hypernovae at early phases (i.e., well before maximum light) both have relatively weak lines in the optical. In the case of Type IIb supernovae, this is because they have hydrogen-dominated atmospheres that when hot (i.e., over of order 10000 K) show weak lines. (Why the lines should be as weak as they are in early Type IIb spectra has not yet been fully elucidated theoretically by NLTE analysis (Baron et al. 1995).) Type Ic hypernovae show weak lines at early times because they are hot (which tends to cause weak optical lines also in cases with little or no hydrogen) and because their velocity structure is very fast giving them extremely broad P-Cygni lines with line velocities of up to 30000 $\mathrm{km\,s^{-1}}$ and perhaps higher (e.g., Mazzali et al. 2000; Patat et al. 2001). The stretching out of P-Cygni lines by very high velocities tends to make them shallower and more overlapping. Both effects tend to give line features a small vertical scale relative to the continuum. If we used f_i's in the formula for DIFF1 instead of δ_i's, the DIFF1 values between early phase spectra of Type IIb's and Type Ic hypernovae would be small even though the spectra and the supernovae are intrinsically quite different because the formula numerators would be relatively small and the formula denominators relatively large. However, the given formula for DIFF1 distinguishes the two types of spectra because the formula denominators become small when the lines features are small.

For our calculations, we interpolated the locally-normalized spectra onto a grid of equally spaced points in (natural) logarithmic wavelength. For coding convenience, we chose $\ln(1\,\text{Å}) = 0$ to be the zero point of the logarithmic wavelength scale. For the grid increment, we chose

$$\Delta \ln(\lambda) = \frac{1}{3000} \ . \tag{15}$$

If the grid wavelengths labeled by i are λ_i and we define $\Delta\lambda_i = \lambda_i - \lambda_{i-1}$, we find that

$$\Delta \ln(\lambda) = \ln(\lambda_i) - \ln(\lambda_{i-1}) = \ln\left(\frac{\lambda_i}{\lambda_{i-1}}\right) = \ln\left(1 + \frac{\Delta\lambda_i}{\lambda_{i-1}}\right) \approx \frac{\Delta\lambda_i}{\lambda_{i-1}} \tag{16}$$

to first order in small $\Delta\lambda_i/\lambda_{i-1}$. We now see that the logarithmic wavelength increment corresponds to a relative change in wavelength for each increment of approximately 1/3000. Thus, near 3000 Å, the wavelength increment is about 1 Å; near 6000 Å, about 2 Å. The Doppler shift velocity corresponding to a relative wavelength increment of 1/3000 is about 100 $\mathrm{km\,s^{-1}}$. As mentioned in § 2.2, supernova line features generally change relatively slowly over wavelength shifts corresponding to velocity changes of order 1000 $\mathrm{km\,s^{-1}}$, and thus our grid should be sufficiently fine for almost all supernova spectra. As also mentioned in § 2.2,

interstellar and telluric lines can vary on shorter wavelength scales, but these are not intrinsic to supernova spectra and could be corrected for if necessary.

We only apply the DIFF1 test to what we call the good overlap region in logarithmic wavelength of two locally-normalized spectra. In this logarithmic wavelength region, both the spectra seem physically good. By physically good, we mean not excessively noisy and not showing unphysical behavior in a narrow wavelength band because of some calibration error. We only allow one good region for a spectrum: i.e., we never multiple good regions for a spectrum which are separated in wavelength. This is not much of a limitation since the bad regions are usually the spectrum ends which can often be very noisy and have narrow wavelength band calibration errors. We only consider DIFF1 tests valid if the good overlap region in logarithmic wavelength is ≥ 0.2 which corresponds to a good overlap region in relative wavelength of $\sim 22\,\%$ relative to the lower wavelength of the region. Since almost all the spectra we consider are good or nearly good over the range 4000–7000 Å (logarithmic wavelength range ~ 0.5596 or relative wavelength range of $75\,\%$ relative to 4000 Å), almost all DIFF1 evaluations are considered valid.

4.2. DIFF2

The DIFF2 formula is

$$\mathrm{DIFF2} = \frac{1}{I} \sum_{i} \frac{|\delta_{1,i} - \delta_{2,i+k}|}{\max\left(|\delta_{1,i}|, |\delta_{2,i+k}|, \xi\right)} \ . \tag{17}$$

The only difference from equation (12) for DIFF1 (§ 4.1) is the term k in the wavelength subscript of one of the flux differences (defined by eq. (11) in § 4.1). This k is chosen to minimize the DIFF2 function value: this minimized value is the DIFF2 value itself. We allow up and down (natural) logarithmic wavelength shifts of only up to 0.05. Thus, we allow up and down relative wavelength shifts of only about $5\,\%$. Given that the logarithmic wavelength grid increment is $\Delta \ln(\lambda) = 1/3000$ (see § 4.1, eq. (15)), it follows that we allow k to vary up and down from zero by $0.05/(1/3000) = 150$. If the minimizing value of k turns out to be one of the k limits -150 or 150, then we consider the test invalid since the true minimizing value of k is almost certainly beyond the k limits. This occasionally happens and indicates the tested spectra are likely not very similar and likely cannot be made to look similar by shifting them relative to each other in logarithmic wavelength: if they can, the resemblance is likely accidental. Also we only consider DIFF2 tests valid if the good overlap region in logarithmic wavelength (which is specified in § 4.1) when the locally-normalized spectra are not relatively shifted (i.e., when $k = 0$) is ≥ 0.2 which corresponds to a good overlap region in relative wavelength of $\sim 22\,\%$ relative to the lower wavelength of the region.

This is the same overlap criterion for validity as used for the DIFF1 test and, as mentioned in § 4.1, is almost always met for spectra we consider.

By its nature, DIFF2 $\leq$ DIFF1 for any spectrum pair. Thus, DIFF2 has an upper limit of 2 like DIFF1 (see § 4.1). But it is even less likely for DIFF2 than for DIFF1 that any value will approach 2. To do that would imply that the locally-normalized spectra were anticorrelated no matter how one shifted them over the allowed shifting range. Since even accidental anticorrelations of spectra in a large sample will tend to be avoided by the shifting, we do not expect DIFF2 values that are well over 1.

We have subjected the set of all possible spectrum pairs drawn from the sample of HDCC supernovae described in § 5 to the DIFF2 test. (There are 17 supernovae, 168 spectra, and 25172 valid spectrum pair tests: some possible pair tests are excluded as invalid by the validity criteria discussed above.) The resulting distribution of DIFF2 values has mean, standard deviation, minimum value, and maximum value of, respectively, 0.784, 0.116, 0.229, and 1.131 (where we have reported more digits than are significant to allow for numerical consistency checks). The mean, minimum, and maximum values are, of course, a bit smaller than the corresponding values for DIFF1 reported in § 4.1: all the DIFF2 values that go into determining these distribution characteristics are equal to or smaller than the corresponding DIFF1 values used to evaluate the distribution characteristics in § 4.1. The standard deviation value shows that spectrum pairs significantly (i.e., 1σ) more alike than average will have DIFF2 values of $\lesssim 0.67$. The maximum value as expected is not well over 1.

The rationale for DIFF2 is as follows. The structure of P-Cygni line profiles in supernovae is correlated with the velocity structure of the ejecta since that velocity structure determines the Doppler shifts of line features. Most noticeably, weak, unblended lines in the photospheric phase tend to have their absorption features reach a minimum at a wavelength shift corresponding to the photospheric velocity (e.g., Jeffery & Branch 1990, p. 188). All parts of the absorption feature have blueshifts that are usually correlated with the photospheric velocity in the sense that the greater the photospheric velocity, the greater the blueshift of each part of the absorption feature: this is just because the whole velocity structure of the line-forming region at any phase tends to be correlated with the photospheric velocity at that phase. In comparing photospheric spectra for similar supernovae, there is often some difference in the width scale of line profiles, particularly the absorption features, attributable to some difference in the velocity structure. The difference may be intrinsic to the supernovae: one supernova may just have layers that move faster than the corresponding layers in the other supernova at the same phase. On the other hand, the difference may just be a matter of phase since the photosphere recedes into the ejecta as time passes because the overall optical depth of the supernova falls. Of course, intrinsic and phase differences in

velocity structure are usually both present to one degree or another.

The eye can usually discern similar line profile patterns despite differing velocity structure. However, the DIFF1 test may not pick out a striking similarity in two spectra seen by the eye because Doppler-shift-caused offsets of line profiles between the two spectra may lead to large contributions to the DIFF1 value. One can imagine compensating for the different velocity structures by a wavelength varying shift, but this seems too complex for practical use. Since the blueshifted absorption features are often larger than the emission features (necessarily the case if the lines are pure scattering (e.g., Jeffery & Branch 1990, p. 189)), a general wavelength shift that tends to align the absorption features may bring out similarities both to the eye and in the DIFF2 test (i.e., by minimizing the DIFF2 function value). Branch et al. (2006a) showed that general shifts were useful in bringing out similarities. We expect that the DIFF2 test shift will usually minimize the DIFF2 function value by tending to align blueshifted absorption features in photospheric phase spectra.

In the nebular phase, the emission lines tend to be symmetric about the rest-frame line-center wavelength. If this is the case, the minimizing shift of the DIFF2 test is likely to be small or zero and DIFF2 will tend to reduce to DIFF1. However, if the emission peaks of one or both locally-normalized spectra are offset from the line-center wavelengths because of some asymmetry in the ejecta, then the DIFF2 test will compensate for that and again bring out similarities that could be missed by the DIFF1 test.

Because DIFF2's logarithmic wavelength shift will often compensate for Doppler shifts caused by differences in velocity structure, it is useful to define a corresponding Doppler shift velocity parameter $v_{\rm param}$ characteristic of the difference in velocity scale between two locally-normalized spectra. We first preliminarily define $v_{\rm param}$ for a wavelength shift $\delta\lambda$ from an initial wavelength λ using the 1st order Doppler formula (eq. (8) in § 2.2, *mutatis mutandis*): thus we have

$$\frac{\delta\lambda}{\lambda} = \frac{v_{\rm param}}{c} \ , \tag{18}$$

where we define positive velocities as giving redshifts. Say the corresponding logarithmic wavelength shift is $\delta\ln(\lambda)$ and recall we only allow logarithmic wavelength shifts of up to 0.05. The allowed logarithmic wavelength shifts are sufficiently small that we can then make the approximation

$$\delta\ln(\lambda) \approx \frac{\delta\lambda}{\lambda} \ . \tag{19}$$

We now give the final definition for $v_{\rm param}$ by combining equations (18) and (19):

$$v_{\rm param} = c\delta\ln(\lambda) \ . \tag{20}$$

4.3. An Example of Two Locally-Normalized Spectra Fitted by Minimizing the DIFF2 Function Value

Figure 6 shows an example of two locally-normalized spectra with the dotted-line spectrum given the logarithmic wavelength shift that minimizes the DIFF2 function value for the two spectra. The solid-line spectrum is the SN 1993J 1993 April 15 spectrum (which comes from about 2 days before UVOIR bolometric maximum light) shown in Figure 2 (§ 3.2) and the dotted-line spectrum is the SN 1987K 1987 August 9 spectrum (Filippenko 1988) (which comes from about 9 days after a red-optical maximum light). In this case, DIFF1 = 0.642 and DIFF2 = 0.612 and the Doppler shift velocity parameter (see definition eq. (20) in § 4.2) corresponding to DIFF2's logarithmic wavelength shift has absolute value $999\,\mathrm{km\,s^{-1}}$. In this case, DIFF2's logarithmic wavelength shift is a blueshift when applied to the SN 1987K spectrum: as noted above we have given this shift to the SN 1987K spectrum in Figure 6. The change from DIFF1 to DIFF2 and the Doppler shift velocity parameter are not large in this case and, in fact, the eye cannot detect any overall improvement in fit in going from a plot without the shift to the plot with it (i.e., Fig. 6). The small change between the DIFF1 and DIFF2 and the small shift is to be expected. First, the spectra both come from Type IIb supernovae. Second, out of our current and preliminary sample of hydrogen-deficient spectra (see § 5), the SN 1987K 1987 August 9 spectrum is the closest match according to DIFF2 to the SN 1993J 1993 April 15 spectrum, except for other spectra from SN 1993J that come from phases close to 1993 April 15. According to DIFF1, it is only the second closest non-SN-1993J match: the SN 1987K 1987 August 7 spectrum is slightly closer with DIFF1 = 0.624.

The phase (day −2) of the SN 1993J spectrum is relative to the well determined UVOIR bolometric maximum light (see §§ 3 and 3.2). The phase (day +9) of the SN 1987K spectrum is relative to a red-optical maximum that is estimated to be 1987 July 31 with an uncertainty of ±4 days (Filippenko 1988). Supernova SN 1993J was a particularly well-observed supernova, and hence our precise knowledge of its phase. Supernova SN 1987K was only moderately well-observed, and hence our uncertainty about its phase and also the light curve from which the phase was determined. The data available for SN 1987K is typical for the supernovae that must dominate any current sample of supernovae for statistical spectral analysis.

The identifications in Figure 6 are the same as in Figure 2 (§ 3.2), except for the residual telluric absorption lines in the SN 1987K spectrum (Filippenko 1988). The region from the blue side of the telluric lines to the red end of the SN 1987K spectrum were excluded from the evaluation of DIFF1/2: i.e., this region was not part of the good overlap region in logarithmic wavelength for the spectrum pair (§§ 4.1 and 4.2).

4.4. Comparing DIFF1 and DIFF2

Both DIFF1 and DIFF2 measure the physical similarity of line formation, and thus of supernovae. DIFF1 puts more weight on overall physical similarity of the supernovae than DIFF2 because the DIFF2 shift in logarithmic wavelength compensates somewhat for some physical distinction in the supernovae. A spectrum pair with very small DIFF1 value may well come from nearly identical supernovae at nearly the same phase. On the other hand, a spectrum pair with a very small DIFF2 value, but not a small DIFF1 value, may well come from supernovae that are in some ways physically alike, but are physically distinct in some other ways.

The most obvious physical distinction that the logarithmic wavelength shift in the DIFF2 test can compensate for is in velocity structure: the distinction is caused either by an intrinsic difference or a phase difference. Another possible distinction is in viewing direction for supernovae that are asymmetric. Note that asymmetric supernovae even if identical would have different spectral evolution depending on viewing angle. There is, in fact, considerable evidence from supernova polarimetry and spectropolarimetry for asymmetry in core-collapse supernovae (e.g., Wheeler & Benetti 2000; Wang et al. 2001; Leonard & Filippenko 2005). One important kind of asymmetry can be parameterized by a major-to-minor axis ratio for characteristic orthogonal axes perpendicular to the line of sight. Spectropolarimetric observations suggest that this axis ratio can vary from 1 to 2 or more (e.g., Wang et al. 2001). For example, the Type IIb supernovae SN 1993J and SN 1996cb spectropolarimetric data suggest an axis ratio of $\gtrsim 1.4$ for both these supernovae (Wang et al. 2001). There are data that suggest, but with considerable uncertainty, that asymmetry increases with decreasing hydrogen envelope mass (Wang et al. 2001; Leonard & Filippenko 2005). Another kind of asymmetry in core-collapse supernovae, that of a jet (or bipolar jets) emerging from the main part of the ejecta, is suggested by the spectropolarimetry of Type Ic hypernova SN 2002ap (Kawabata et al. 2002; Leonard et al. 2002). Type Ia supernovae also show polarization in some cases: the polarization may arise from clumps in the ejecta (e.g., Leonard et al. 2005).

Because of the use of local normalization, both DIFF1 and DIFF2 tests are useful for studying supernovae which frequently have uncertain continua.

5. A PRELIMINARY STATISTICAL ANALYSIS OF HYDROGEN-DEFICIENT CORE-COLLAPSE SUPERNOVA SPECTRA

We are beginning a project of comparative analysis of the spectra of HDCC supernovae (i.e., hydrogen-deficient core-collapse supernovae of Types IIb, Ib, Ic, and Ic hypernovae: see

§ 1) that will include a statistical analysis of the spectra as well a spectral modeling using the parameterized spectrum-synthesis code SYNOW (e.g., Branch et al. 2003, 2005, and references therein). We note that Types IIb, Ib, and Ic seem to be a sequence of decreasing hydrogen and helium in the supernova ejecta. Type Ib supernovae have conspicuous helium lines, but not conspicuous hydrogen lines. Type IIb supernovae have conspicuous, but weak hydrogen lines and resemble Type Ib supernovae. Type Ic supernovae lack conspicuous hydrogen lines and conspicuous helium lines. As mentioned in the § 1, Type Ic hypernovae are particularly energetic Type Ic supernovae that in some cases are associated with GRBs: e.g., SN 1998bw with GRB 980425 (e.g., Galama et al. 1998). All the core-collapse supernovae lack the strong Si II λ6355 line that characterizes Type Ia supernovae. The spectral classification of supernovae is well reviewed by Filippenko (1997), but note that this paper precedes the discovery of Type Ic hypernovae.

We need to make clear that the HDCC supernova types are not completely distinct and the determination of whether particular lines are conspicuous or not is sometimes ambiguous. For example, relatively inconspicuous hydrogen lines do seem to be present in Type Ib supernovae (e.g., Branch et al. 2002), and so drawing the line between Type IIb's and Type Ib's cannot always be clear. Likewise there is sometimes difficulty in distinguishing Type Ib's from Type Ic's and some supernovae that cannot be clearly set in either category are often classified as Type Ibc supernovae. On the other hand, the work of Matheson et al. (2001) shows that the distinction between Type Ib's and Type Ic's is strong enough to continue requiring the two types rather than a single merged type.

To undertake the HDCC supernova analysis project, we are assembling HDCC supernova spectra in html files in supernova directories at SUSPEND (see § 1) under the heading *Supernovae by Epoch*. The spectrum files have header information about the spectra and the supernovae they come from. Plots of the spectra in original form and locally-normalized form are also given in the headers. The original spectra follow the header in two-column format: the columns being wavelength and flux. The locally-normalized spectra are given in the dif subdirectories of the supernova directories. A list of the spectra are currently in html files (including those spectra from non-HDCC supernovae) can be found under the heading *Lists* at SUSPEND.

At present, we are at a very early stage in the project and have not assembled many of the spectra available for HDCC supernovae nor determined the best way to proceed with our statistical analysis. However, to illustrate the use of DIFF1 and DIFF2, we present some preliminary results.

5.1. Table 1 and Tables at SUSPEND

Table 1 gives some statistics on the HDCC supernovae and spectra we have assembled so far in SUSPEND (see § 1). As one can see from the table, there are currently 17 supernovae and 168 spectra in the sample. The supernovae include the prototype Type Ib supernovae SN 1983N and SN 1984L (Harkness et al. 1987) and the well-observed Type Ic's SN 1987M (Filippenko et al. 1990) and prototypes. SN 1994I (e.g., Clocchiatti et al. 1996). The peculiar Type Ibc SN 2005bf (e.g., Folatelli et al. 2006; Parrent et al. 2007) is included as well: this supernova had two observed maxima, had a rise time of about 40 days to the second and main optical maximum (typical Type Ib/c rise times are of order 20 days), and was unusually luminous. (Supernovae also have a near-explosion maximum light that is almost never observed, and so usually unmentioned. This is not the maximum light we refer to here as the first maximum light of SN 2005bf.) SN 2005bf also made a transition from Type Ic to Type Ib behavior in the period from about day −30 to about day +20 relative to the (main) optical maximum (e.g., Folatelli et al. 2006): because of this transition, SN 2005bf is classified as a Type Ibc. Only two Type IIb supernovae have been included so far: the already discussed prototype SN 1987K (§ 4.3; Filippenko 1988) and the very well-observed SN 1993J (§ 3 and § 4.3; e.g., Jeffery et al. 1994; Richmond et al. 1994; Baron et al. 1995; Clocchiatti et al. 1995; Houck & Fransson 1996; Fransson et al. 2005). Three Type Ic hypernovae are included: SN 1997ef (e.g., Mazzali et al. 2000), SN 1998bw (e.g., Galama et al. 1998; Iwamoto et al. 1998; Patat et al. 2001), and SN 2002ap (e.g., Kawabata et al. 2002; Leonard et al. 2002; Foley et al. 2003). Also included are less famous HDCC supernovae observed by Matheson et al. (2001) and others.

In the calculations described below, we included only one spectrum for each phase period (which we usually set to being 1 day) from each supernova. The other spectra for that phase period are redundant since they should be nearly identical to the included spectrum aside from observational error. The spectrum we included is the one we deem to be best: this is usually because of broader wavelength coverage.

In an automated fashion, we have calculated DIFF1 and DIFF2 for all supernova spectrum pairs in the sample: these spectrum pair DIFF1/2 values can be found tabulated at SUSPEND under the heading *Lists*. For each spectrum, there is a table listing all other spectra in order of increasing DIFF1/2 values relative to it. These tables are updated as more supernovae and spectra are added to the sample. We have excluded from the analysis below and in § 5.2 those DIFF1 and DIFF2 values deemed invalid by the rules discussed in §§ 4.1 and 4.2.

As well as ordering spectra in order of likeness using DIFF1/2 values, we want some way to order supernovae in order of likeness. As a preliminary method, for any two supernovae

we calculate all (valid) DIFF1/2 values between spectrum pairs with one of the pair coming from one supernova and the other from the other supernova: i.e., we calculate the non-self spectrum pair DIFF1/2 values. The smallest of these DIFF1/2 values we call the supernova pair DIFF1/2 value.

The rationale for the definition for supernova pair DIFF1/2 value is as follows. The spectral phase coverage for all supernovae is incomplete (although for some the coverage is very good) and rarely are both supernovae covered at a common phase to within a day: often coverage at even a nearly common phase is lacking. Also phase measured from a time zero set at maximum light (which is how we define phase following a common convention) is itself uncertain. Ideally, one would like to use an accurate UVOIR bolometric maximum light as time zero for supernova phase. We do that when an accurate UVOIR bolometric maximum light is available (which is rarely). Usually, however, we must use a substitute which is often some optical broad-band maximum light. These broad-band maxima usually happen within a few days of UVOIR bolometric maximum light and have some uncertainty. In some cases, all we can use as a substitute is what can be loosely called optical maximum light which is a fiducial time within a few days of when exact UVOIR bolometric maximum light probably occurs. And in some of these cases, the estimate of optical maximum light is just the day of discovery: supernovae tend to be discovered near or at optical maximum light since that is when they are most readily discoverable because, of course, they are brightest or nearly brightest in all optical bands at optical maximum light. (Throughout the rest of this section we usually do not specify the kind of maximum light we use to set the phase zero point. We usually just refer to all kinds of maximum light as maximum light without qualification.) By choosing the smallest DIFF1/2 value out of all the non-self spectrum pair values for the supernova pair DIFF1/2 value, we hope to have partially avoided the problems of incomplete spectral phase coverage and inaccurate phase measured from UVOIR bolometric maximum light. We assume that the intrinsic likeness of each supernova pair is well measured by their closest observed spectral approach to each other: i.e., what we call the supernova pair DIFF1/2 value. Obviously, because of the incomplete phase coverage, the closest observed spectrum approach may only give a lower limit on likeness. For two supernovae that are actually much alike with at least one having good phase coverage, the closest spectrum approach is probably for the spectrum pair that has the least relative phase difference where in this case phase is measured relative to explosion. (As supernovae evolve from time zero at explosion, their relative rate of spectral evolution tends to be more constant than their absolute rate of spectral evolution.) For two supernovae that are not much alike or that both have poor phase coverage, the closest spectrum approach may not occur for the spectrum pair that has the least or even small relative phase difference.

There are, in fact, cases where two supernovae have a relatively small supernova pair

DIFF1/2 value and yet are in some respects quite different. For example, the day +4 (relative to B maximum) spectrum of Type Ibc SN 1999ex (Hamuy et al. 2002; Stritzinger et al. 2002) is very similar to the day −20 (relative to UVOIR bolometric maximum light) spectrum of Type Ibc SN 2005bf (Folatelli et al. 2006; Parrent et al. 2007). Figure 10 of Parrent et al. (2007) shows overlapping locally-normalized versions of these spectra: to the eye their fit is very close. (See also Fig. 5 of Folatelli et al. 2006.) The supernova pair DIFF1 and DIFF2 values are, respectively, 0.447 and 0.442: these are quite small DIFF1/2 values for spectra from different supernovae as our experience shows. Although SN 1999ex and SN 2005bf are both Type Ibc supernovae, they are quite different in some respects: e.g., rise time to optical maximum: probably of order 20 days for SN 1999ex (Richardson et al. 2006) and about 40 days to the second and main optical maximum, as mentioned above, for SN 2005bf. Also the two closely matching spectra come from very different phases which would not be true if the supernovae were really very much alike: the most closely matching spectra would then tend to come from nearly the same phase. Thus, it is clear that our assumption of intrinsic supernova likeness being well measured by the supernova DIFF1/2 pair is not always valid. However, since our analysis here is preliminary, we leave the search for a better measure of supernova likeness to future work *sine die*.

The tables giving the spectrum pair DIFF1/2 values at SUSPEND (which altogether are quite lengthy) are preceded by tables of supernova pair DIFF1/2 values. For each supernova there is a table listing all other supernovae in order of increasing supernova pair DIFF1/2 values relative it.

5.2. Table 2 and the Standard HDCC Supernova Types

Since this paper is just a beginning in our project of statistical analysis of HDCC supernova spectra, we will not fully discuss the significance of either the tabulated supernova or spectrum pair DIFF1/2 values at SUSPEND (see § 5.1). But as a preliminary investigation, we consider if the classification of HDCC supernovae into Type IIb's, Type Ib's, Type Ic's, and Type Ic hypernovae is discoverable from supernova pair DIFF1/2 values. (Supernovae classified as Type Ibc are grouped with the Type Ib's. There are only two of these in the current sample: SN 1999ex (Hamuy et al. 2002; Stritzinger et al. 2002) and SN 2005bf (e.g., Folatelli et al. 2006; Parrent et al. 2007).) A priori, it is not clear that the HDCC supernova types will be picked out by an analysis with DIFF1/2. The Types IIb, Ib, and Ic, and, in part, the Type Ic hypernova are characterized by particular lines. DIFF1/2 measures overall differences between spectra.

For the preliminary investigation, we have calculated the mean supernova pair DIFF1/2

values between supernovae of different types (the cross-type means) and the mean supernova pair DIFF1/2 values between supernovae of the same type (the self-type means). We have also calculated the estimated standard deviations of the distributions of the supernova pair DIFF1/2 values about the type means using the ordinary standard deviation formula with the correction for using the mean of the sample (e.g., Bevington 1969, p. 19). The standard deviation for the Type IIb self-type mean is assigned a zero value since there are only two Type IIb's in the current sample, and thus only one supernova pair DIFF1/2 value: the standard deviation of the sample is zero; that of the distribution is unknown.

Since HDCC supernovae tend to look increasingly alike as time from explosion (i.e., phase) increases, we have repeated the DIFF1/2 calculations including only supernova pair DIFF1/2 values obtained from spectra that are both from phases less than 10 days past maximum light. The supernova pair DIFF1/2 type means obtained in this case are phase-restricted. We were interested in seeing if phase-restricted approach would better distinguish HDCC supernovae into the standard types than the phase unrestricted approach. Note that phase-unrestricted supernova pair DIFF1/2 values will, of course, always be smaller than or equal to their counterpart phase-restricted supernova pair DIFF1/2 values. (The last remark assumes that counterpart phase-restricted supernova pair DIFF1/2 values exist. They may not if one or both of the supernovae in the pair lack any spectra for the period allowed by the phase restriction.)

The results of all the calculations are given in Table 2 in the form of a type DIFF1/2 correlation matrix consisting of self-type means (the diagonal elements) and cross-type means (the off-diagonal elements): phase-unrestricted DIFF1 values are in Table 2(a), phase-unrestricted DIFF2 values are Table 2(b), phase-restricted DIFF1 values are in Table 2(c), and phase-restricted DIFF2 values are in Table 2(d). The matrix is, of course, symmetric.

Several remarks can be made about the results in Table 2. First, none of the mean values are very small: the smallest is 0.455 which is the Type Ic hypernova DIFF2 self-type mean in Table 2(b). An examination of the table of the phase-unrestricted supernova pair DIFF1/2 values at SUSPEND shows that none are less 0.4: the smallest DIFF1 is 0.418 for the pair of Type Ib SN 1988L and Type Ic SN 1990B; the smallest DIFF2 is 0.409 for the same pair of supernovae and obtained using the same spectrum pair. The fact that these smallest DIFF1/2 values are for supernovae of different assigned types shows that supernova pair DIFF1/2 values are not perfect in discriminating Type Ib and Type Ic supernovae. Some of the spectrum pair DIFF1/2 values are significantly smaller (some below 0.3 going down to minimum values of 0.244 for DIFF1 (see § 4.1) and 0.229 for DIFF2 (see § 4.2)), but those are for spectra from the same supernova usually taken close together in phase. The upper limit on the phase-unrestricted supernova pair DIFF1 values is 0.886 and on the

phase-unrestricted supernova pair DIFF2 values is 0.809. These upper limits were both for the supernova pair of Type Ic SN 1990aa and Type Ib SN 1999di, but not using the same spectrum pair. The supernovae of this pair are not much alike in the phases for which spectra are available.

Second, a mean DIFF2 value is always less than or equal to the corresponding mean DIFF1 value as it must be according to our formulae (§ 4.1, eq. (12) and § 4.2, eq. (17)), but always by less than the standard deviation of the mean DIFF1 value. We have to conclude that DIFF2 is not finding great similarities that are being totally missed by DIFF1.

Third, the phase-restricted mean DIFF1/2 values (in Table 2(c) and Table 2(d)) are all larger than the corresponding phase-unrestricted mean DIFF1/2 values (in Table 2(a) and (b)). This is understandable for two causes. First, HDCC supernovae are qualitatively understood to be more diverse at earlier times, and thus the phase-restricted DIFF1/2 values should tend to be larger. Second, the incompleteness of the phase coverage of a supernova may be greatly increased by phase restriction. Phase restriction reduces the chances of finding supernova pair DIFF1/2 values for the aforementioned supernova with another supernova with pair spectra from nearly the same phase when the spectra would tend to be most alike if the pair supernovae were alike. The effects of the two causes could be sorted out in a more detailed analysis. It is possible for the mean DIFF1/2 values to be reduced by phase restriction. This would happen if phase restriction eliminated a supernova altogether from those going into calculation of the means and that supernova was sufficiently remote from other supernovae to increase phase-unrestricted mean DIFF1/2 values when included. This actually happened in an earlier calculation for the Type Ic self-type means. The phase-restriction eliminates Type Ic SN 1990aa for which no spectra from before 10 days after maximum light are currently available to us. SN 1990aa may be something of an outlier among Type Ic's, and so its inclusion seems to increase the self-type mean DIFF1/2 values. When the sample of Type Ic's was changed this reduction on phase restriction disappeared.

Fourth, the self-type means in any row are the smallest means in that row in all cases. This shows that a DIFF1/2 analysis can probably identify the standard HDCC supernova types on average. If one is given spectra from a new HDCC supernova of unknown type and uses those spectra to find mean supernova pair DIFF1/2 values with samples of the standard types, the smallest mean supernova pair DIFF1/2 value will probably be with the sample of the type to which the new HDCC supernova belongs.

In the rows for Type IIb's and Type Ic hypernovae, the self-type means are smaller than the respective row cross-type means by $\gtrsim 1.5\sigma_{\rm larger}$ in all cases and by $\gtrsim 2\sigma_{\rm larger}$ in all but two cases. (The $\sigma_{\rm larger}$ is the larger of the standard deviations for the two means being compared.) The two cases where difference is less than $2\sigma_{\rm larger}$ are for the DIFF1 and DIFF2

phase-unrestricted Type Ic hypernovae cross-type with the Type Ic's. Overall, Type IIb and Type Ic hypernova are found to be quite distinct from other types.

On the other hand, in the phase-unrestricted rows for Type Ib/Ibc's and phase-unrestricted and phase-restricted rows for Type Ic's the self-type means are smaller than the respective row cross-type means by $\lesssim \sigma_{\rm larger}$. For the phase-restricted cases, the Type Ib/Ibc self-type means in are some cases separated by more than $\sigma_{\rm larger}$ from the Type Ib/Ibc row cross-type means. Overall, one must conclude that Type Ib/Ibc and Type Ic are not as distinct from other types as are Type IIb and Type Ic hypernova. This means that Type Ib/Ibc and Type Ic are more heterogeneous and overlap more in behavior with other types than Type IIb and Type Ic hypernova.

Recall that we introduced phase restriction to see if it would better distinguish HDCC supernovae into the standard types than the phase unrestricted approach. From the results discussed in the last two paragraphs, there is some improvement in distinguishing the types. However, this improvement is rather modest for the particular phase restriction we used: i.e., restricting spectra used to those from before 10 days after maximum light. Maybe other phase restrictions would give greater improvement. This could be investigated in future work.

To finish our preliminary analysis, we note that the Type IIb's and Type Ic hypernovae included in the sample are all relatively well-observed supernovae, and so they suffer relatively little from lack of phase coverage. Some of the Type Ib/Ibc's and Type Ic's in the sample have poor or very poor phase coverage. (See the list of supernova spectra in html format under the heading *Lists* at SUSPEND for the spectra currently available for individual supernovae and the spectrum phases.) The supernova pair DIFF1/2 values for supernovae where both supernovae have poor phase coverage could be large even if the supernovae were very similar simply because the procedure for determining the supernova pair DIFF1/2 values may not be able to find spectra from nearly the same phase. In future work, we will try to remedy this deficiency in the procedure perhaps by giving lower weight in calculating mean DIFF1/2 values to supernova pair DIFF1/2 values from supernova pairs where both members of the pair have poor phase coverage or by using some quite different definition of supernova pair DIFF1/2 value.

6. CONCLUSIONS AND DISCUSSION

We have developed two tests DIFF1 and DIFF2 for measuring goodness-of-fit between two supernova spectra (see § 4.1, eq. (12) and § 4.2, eq. (17) for the formulae). The tests rely

on local normalization (§ 2) which eliminates the uncertainty in the spectrum continuum, except for contamination from extraneous sources (§ 1). Local normalization also eliminates real information stored in continuum shape. However, a basic premise of this paper is that line pattern is a much better signature of intrinsic supernova behavior than continuum shape, and so eliminating continuum shape information is not too important for spectrum comparisons (§ 1).

We have presented some examples of locally-normalized spectra for SN 1993J and given some analysis of the spectra (§ 3). The UV parts of two of the SN 1993J spectra are hitherto unpublished *HST* spectra. In § 3.5, we have shown that local normalization is sufficiently continuum-independent to lead to valid results in comparing locally normalized spectra. One must, however, apply the same local normalization procedure to all original spectra in order to obtain locally-normalized spectra that can be validly compared.

As an example of the use of DIFF1/2, we have used them in a preliminary statistical analysis of the spectra of HDCC (hydrogen-deficient core-collapse) supernovae (§ 5). The analysis shows that standard HDCC supernova types (IIb, Ib/Ibc, Ic, and Ic hypernova) do form distinct groups when compared using DIFF1/2 (§ 5.2). This analysis is preliminary since many available HDCC supernovae and HDCC supernova spectra are not included in the analysis sample. Also many improvements in our statistical procedure are possible.

Tables of all spectrum and supernova pair DIFF1/2 values for our sample of HDCC supernovae are available at the SUSPEND database (see the footnote to the abstract for the URL) under the heading *Lists*. The spectra we have used are also online at SUSPEND in two-column format under the heading *Supernovae by Epoch* in supernova directories in html files along with figures of the original and locally-normalized spectra. The locally-normalized versions of the spectra themselves can be found in the dif subdirectories of the supernova directories.

Although hundreds of supernovae are now being discovered per year (e.g., 367 in 2005 and 526 in 2006 (Central Bureau for Astronomical Telegrams 2007) which gives discovery rates of more than 1 supernova per day), most of these are remote and are relatively poorly observed. Their main use is as cosmological distance indicators and for the determination of supernova rates. New well-observed supernovae accumulate slowly with only a few per year. These new well-observed ones and the past well-observed ones are only relatively well-observed in most cases. Phases are missing, calibrations imperfect, and frequently the reddening correction is very uncertain. Thus, for the foreseeable future, statistical analyses of supernova spectra will have to rely on heterogeneous data sets for relatively few well-observed supernovae. We believe that DIFF1 and DIFF2 (which eliminate the need for accurate continuum shape and that can, in the case of DIFF2, compensate somewhat for

varying phase, velocity structure, and asymmetry (§ 4.4)) will be useful tools in statistical analyses of available spectra.

Another, and not-distinct, use for DIFF1/2 is to find for new and, perhaps, not-well-observed supernovae, well-observed supernovae that are their near-twins. Then insofar as the well-observed supernovae are understood, the new supernovae will be understood.

DIFF1/2 should also be useful in synthetic spectrum analysis of supernova spectra because, again, it eliminates the uncertain continuum of observed supernovae. Certainly fitting the true continuum is one of the goals and guides in achieving a good synthetic spectrum fit to the observations. But when the fitting exercise gives a good fit to an incorrect continuum, then the fitting exercise becomes misleading. A good fit to the lines with highly realistic radiative transfer and a realistic hydrodynamic model should yield a good continuum and that should allow one to correct the observed continuum for errors in dereddening and calibration.

The future of synthetic spectrum modeling of supernovae may well be the calculation of time-dependent radiative transfer for a large collection of realistic hydrodynamic models that span many possible explosion outcomes. As time passes more models will be included in the collection and the realism of the models and the radiative transfer will be improved. Eventually, almost all old and new supernovae could find a near-twin in the collection using some test like DIFF1/2 and will then be well understood. This ideal situation is still far off, but there is work heading toward it (e.g., Woosley et al. 2007, for Type Ia supernovae).

In future work, we plan to use DIFF1/2 in fuller statistical analyses of HDCC supernova spectra than that presented in this paper. These analyses will also include spectral modeling using the parameterized spectrum-synthesis code SYNOW (e.g., Branch et al. 2003, 2005, and references therein). Use of DIFF1/2 for other supernova types is also envisaged for future work.

We would like to thank all the observers who obtained the spectra used in this paper, Peter Challis (who prepared the two nebular-phase *HST* spectra for us some time ago) and Stéphane Blondin for information about some of the SN 1993J spectra we present, and the referee for his/her comments. Support for this work has been provided by NASA grant NAG5-3505 and the Homer L. Dodge Department of Physics & Astronomy of the University of Oklahoma.

REFERENCES

Barbon, R., Benetti, S., Cappellaro, E., Patat, F., Turatto, M., & Iijima, T. 1995, A&AS, 110, 513

Barbon, R., Ciatti, F., Rosino, L., Ortolani, S., & Rafanelli, P. 1982, A&AS, 116, 43

Baron, E., Hauschildt, P. H., Branch, D., Austin, S., Garnavich, P., Ann, H. B., Wagner, R. M., Filippenko, A. V., Matheson, T., & Liebert, J. 1995, ApJ, 441, 170

Baron, E., Nugent, P. E., Branch, D., & Hauschildt, P. H. 2004, ApJ, 616, L91

Baron, E., Nugent, P. E., Branch, D., & Hauschildt, P. H. 2005, in 1604-2004: Supernovae as Cosmological Lighthouses, ASP Conference Series, Vol. 342, Proceedings of the conference held 15–19 June, 2004 in Padua, Italy, ed. M. Turatto, S. Benetti, L. Zampieri, & W. Shea (San Francisco: Astronomical Society of the Pacific), 351, astro-ph/0409659

Baron, E., Nugent, P. E., Branch, D., Hauschildt, P. H., Turatto, M., & Cappellaro, E. 2003, ApJ, 586, 1199

Beals, C. S. 1931, MNRAS, 91, 966

Bevington, P. R. 1969, Data Reduction and Error Analysis for the Physical Sciences (New York: McGraw-Hill Book Company)

Blondin, S. 2007, private communication

Blondin, S., & Tonry, J. L. 2007, in The Multicoloured Landscape of Compact Objects and their Explosive Origins, Cefalù, Sicily, 2006 June 11—24, ed. L. Burderi et al. (Melville, New York: American Institute of Physics), in press, astro-ph/0612512

Branch, D., Baron, E., Hall, N., Melakayil, M., & Parrent, J. 2005, PASP, 117, 545

Branch, D., Jeffery, D. J., Young, T. R., & Baron, E. 2006a, PASP, 118, 791

Branch, D., et al. 2002, ApJ, 566, 1005

Branch, D., et al. 2003, AJ, 126, 1489

Branch, D., et al. 2006b, PASP, 118, 560

Buta, R. J. 1982, PASP, 94, 578

Cardelli, J. A., Clayton, G. C., & Mathis, J. S. 1989, ApJ, 345, 245

Central Bureau for Astronomical Telegrams 2007, (Cambridge, Massachusetts: Center for Astrophysics), http://cfa-www.harvard.edu/iau/cbat.html

Challis, P. 1994, private communication

Challis, P. 2006, private communication

Chugai, N. N. 1988, Sov. Astron. Lett., 14(5), 334

Clocchiatti, A., Wheeler, J. C., Barker, E. S., Filippenko, A. V., Matheson, T., & Liebert, J. W. 1995, ApJ, 446, 167

Clocchiatti, A., Wheeler, J. C., Brotherton, M. S., Cochran, A. L., Wills, D., Barker, E. S., & Turatto, M. 1996, ApJ, 462, 462

Dessart, L., & Hillier, D. J. 2005, A&A, 437, 667

Filippenko, A. V. 1988, AJ, 96, 1941

Filippenko, A. V. 1997, ARA&A, 35, 309

Filippenko, A. V. 1994, private communication

Filippenko, A. V., & Matheson, T. 1993, IAU Circ. 5787

Filippenko, A. V., Porter, A. C., & Sargent, W. L. W. 1990, AJ, 100, 1575

Folatelli, G., et al. 2006, ApJ, 641, 1039

Foley, R. J. 2003, PASP, 115, 1220

Fransson, C. 1982, A&A, 111, 140

Fransson, C. 1984a, A&A, 132, 115

Fransson, C. 1984b, A&A, 133, 264

Fransson, C., Benvenuti, P., Wamsteker, W., Gordon, C., Hempe, K., Reimers, D., Palumbo, G. G. C., & Panagia, N. 1984c, A&A, 132, 1

Fransson, C., Lundqvist, P., & Chevalier, R. A. 1996, ApJ, 461, 993

Fransson, C. et al. 2005, ApJ, 622, 991

Freedman, W. L., et al. 1994, ApJ, 427, 628

Galama, T., et al. 1998, Nature, 395, 670

Hamuy, M., et al. 2002, AJ, 124, 417

Harkness, R. P., et al. 1987, ApJ, 317, 355

Harutyunyan, A., Benetti, S., Cappellaro, E., & Turatto, M. 2005, in ASP Conf. Ser. 342, 1604–2004: Supernovae as Cosmological Lighthouses, ed. M. Turatto, S. Benetti, L. Zamperi, & W. Shea (San Francisco: ASP), 258

Houck, J. C., & Fransson, C. 1996, ApJ, 456, 811

INES (*IUE* Newly Extracted Spectra) 2000, The INES Archive Data Server, Version 3.0: *IUE* Final Archive (Villafranca del Castillo, Spain: Laboratory for Space Astrophysics and Theoretical Physics), http://iuearc.vilspa.esa.es/ines/index2.html

Iwamoto, K., et al. 1998, Nature, 395, 672

Jeffery, D. J. 1993, ApJ, 415, 734

Jeffery, D. J., & Branch, D. 1990, in Jerusalem Winter School for Theoretical Physics, Vol. 6, Supernovae, ed. J. C. Wheeler, T. Piran, & S. Weinberg (Singapore: World Scientific), 149

Jeffery, D. J., et al. 1994, ApJ, 421, L27

Kawabata, K., et al. 2002, ApJ, 580, L39

Kirshner, R. P., Blades, J. C., Branch, D., Chevalier, R. A., Fransson, C., Panagia, N., Wagoner, R. V., & Wheeler, J. C. 1988, *HST* Proposal SINS: The Supernova INtensive Study, unpublished

Kirshner, R. P., et al. 1993, ApJ, 415, 589

Lawden, D. F. 1975, An Introduction to Tensor Calculus and Relativity (London: Chapman and Hall)

Leonard, D. C., & Filippenko, A. V. 2005, in 1604-2004: Supernovae as Cosmological Lighthouses, ASP Conference Series, Vol. 342, Proceedings of the conference held 15–19 June, 2004 in Padua, Italy, ed. M. Turatto, S. Benetti, L. Zampieri, & W. Shea (San Francisco: Astronomical Society of the Pacific), 330, astro-ph/0409659

Leonard, D. C., Filippenko, A. V., Chornock, R., & Foley, R. J. 2002, PASP, 114, 1333

Leonard, D. C., Li, W., Filippenko, A. V., Foley, R. J., & Chornock, R. 2005, ApJ, 632, 450

Matheson, T., Filippenko, A. V., Li, W., Leonard, D. C., & Shields, J. C. 2001, AJ, 121, 1648

Matheson, T., et al. 2003, ApJ, 599, 394

Mazzali, P. A., Iwamoto, K., Nomoto, K. 2000, ApJ, 545, 407

Mihalas, D. 1978, Stellar Atmospheres, (San Francisco: W. H. Freeman and Company)

Moore, C. E., & Merrill, P. W. 1968, in NSRDS–NBS 23, Partial Grotrian Diagrams of Astrophysical Interest (Washington, DC: Government Printing Office), http://www.nist.gov/srd/nsrds.htm

NIST (National Institute of Standards and Technology) 2006, NIST Atomic Spectra Database Version 3.1.0 (Gaithersberg, Maryland: NIST), http://physics.nist.gov/PhysRefData/ASD/

O'Donnell, J. E. 1994, ApJ, 422, 158

Panagia, N. et al. 1980, MNRAS, 192, 861

Parrent, J., Branch, D., Troxel, M. A., Casebeer, D., Jeffery, D. J., Ketchum, W., Baron, E. Serduke, F. J. D., & Filippenko, A. V. 2007, PASP, 119, 135

Patat, F., et al. 2001, ApJ, 555, 900

Paturel, G., Petit, C., Prugniel, Ph., Theureau, G., Rousseau, J., Brouty, M., Dubois, P., & Cambrésy, L. 2003, A&A, 412, 45, http://leda.univ-lyon1.fr/

Phillips, M. M., et al. 1987, PASP, 99, 592

Pun, C. S. J., et al. 1995, ApJS, 99, 223

Qiu, Y., Li, W., Qiao, Q., & Hu, J. 1999, AJ, 117, 736

Reichard, T. A., et al. 2003, AJ, 125, 1711

Richardson, D., Branch, D., & Baron, E. 2006, AJ, 131, 2233

Richmond, M. W., Treffers, R. R., Filippenko, A. V., Paik, Y., Leibundgut, B., Schulman, E., & Cox, C. V. 1994, AJ, 107, 1022

Ripero, J. 1993, IAU Circ. 5731

Ruiz-Lapuente, P., Kirshner, R. P., Phillips, M. M., Challis, P. M., Schmidt, B. P., Filippenko, A. V., & Wheeler, J. C. 1995, ApJ, 439, 60

Schlegel, D. J., Finkbeiner, D. P., & Davis, M. 1998, ApJ, 500, 525

Stritzinger, M. et al. 2002, AJ, 124, 2100

Wamsteker, W., Rodriguez, P. M., Gonzalez, R., Sonneborn, G., & Kirshner, R. P. 1993, IAU Circ. 5738

Wang, L., Howell, D. A., Höflich, P., & Wheeler, J. C. 2001, ApJ, 550, 1030

Weiler, K. W., Sramek, R. A., Panagia, N., van der Hulst, J. M., & Salvati, M. 1986, ApJ, 301, 790

Wheeler, J. C., & Benetti, S. 2000, in Allen's Astrophysical Quantities, 4th Edition, ed. A. N. Cox (New York: Springer-Verlag; AIP), 451

Wheeler, J. C., et al. 1993, ApJ, 417, L71

Wiese, W. L., Smith, M. W., & Glennon, B. M. 1966, in NSRDS–NBS 4, Atomic Transition Probabilities: Vol. I—Hydrogen through Neon (Washington, DC: Government Printing Office)

Wiese, W. L., Smith, M. W., & Miles, B. M. 1969, in NSRDS–NBS 22, Atomic Transition Probabilities: Vol. 2—Sodium through Calcium (Washington, DC: Government Printing Office)

Woosley, S. E., Kasen, D., Blinnikov, S., & Sorokina, E. 2007, ApJ, in press, astro-ph/0609562

Woosley, S. E., Pinto, P. A., Martin, P. G., & Weaver, T. A. 1987, ApJ, 318, 664

This preprint was prepared with the AAS LaTeX macros v5.2.

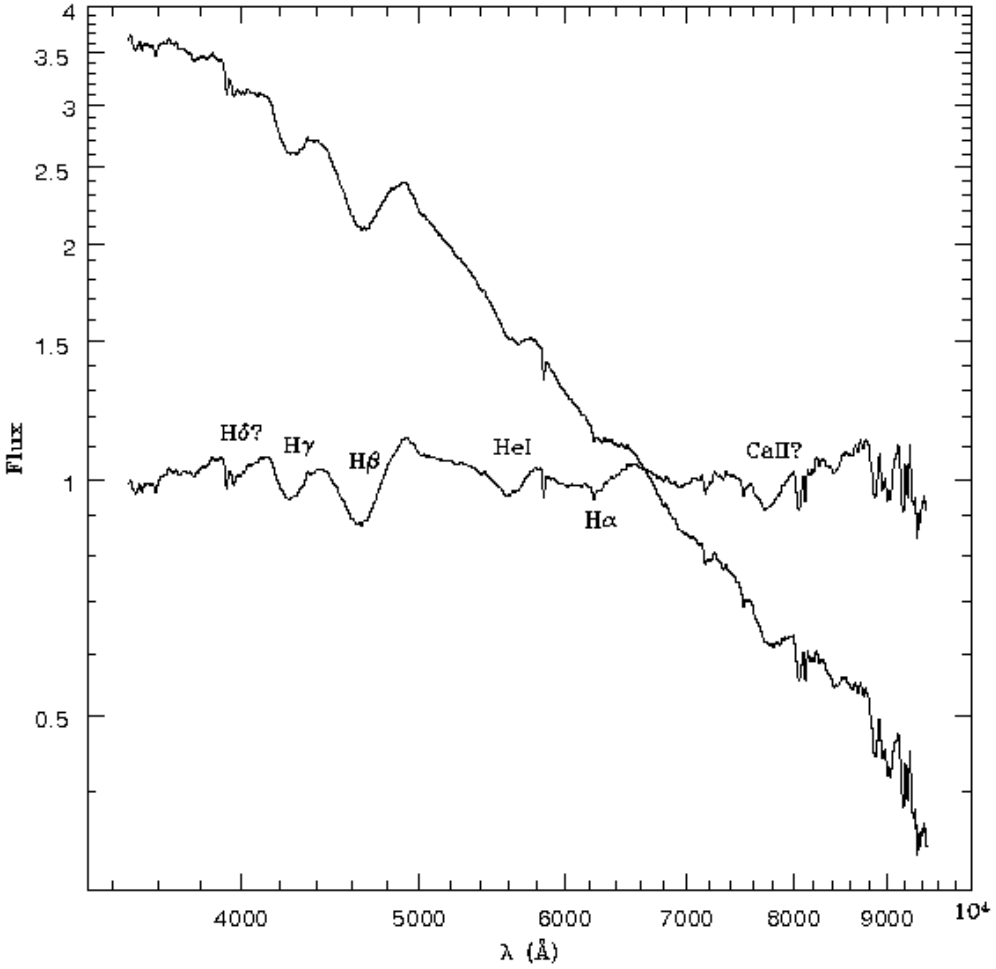

Fig. 1.— The spectrum of Type IIb SN 1993J in the f_λ and locally-normalized representations from 1993 March 31 which is about 16 days before UVOIR bolometric maximum light and about 4 days after explosion. The locally-normalized spectra in this and in other figures are obviously the ones with continuum level of about 1.

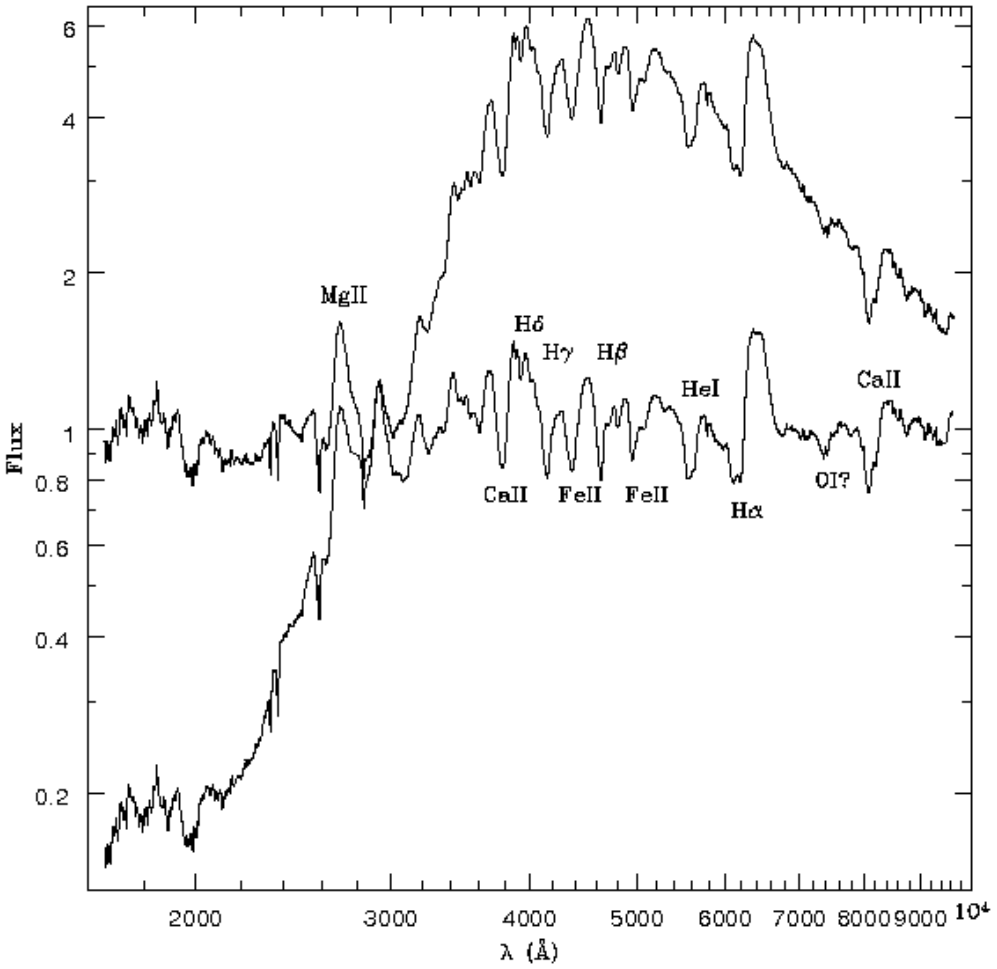

Fig. 2.— The spectrum of Type IIb SN 1993J in the f_λ and locally-normalized representations from 1993 April 15 which is about 2 days before UVOIR bolometric maximum light and 18 days after explosion. From 3240 Å blueward, the spectrum is an *HST* spectrum.

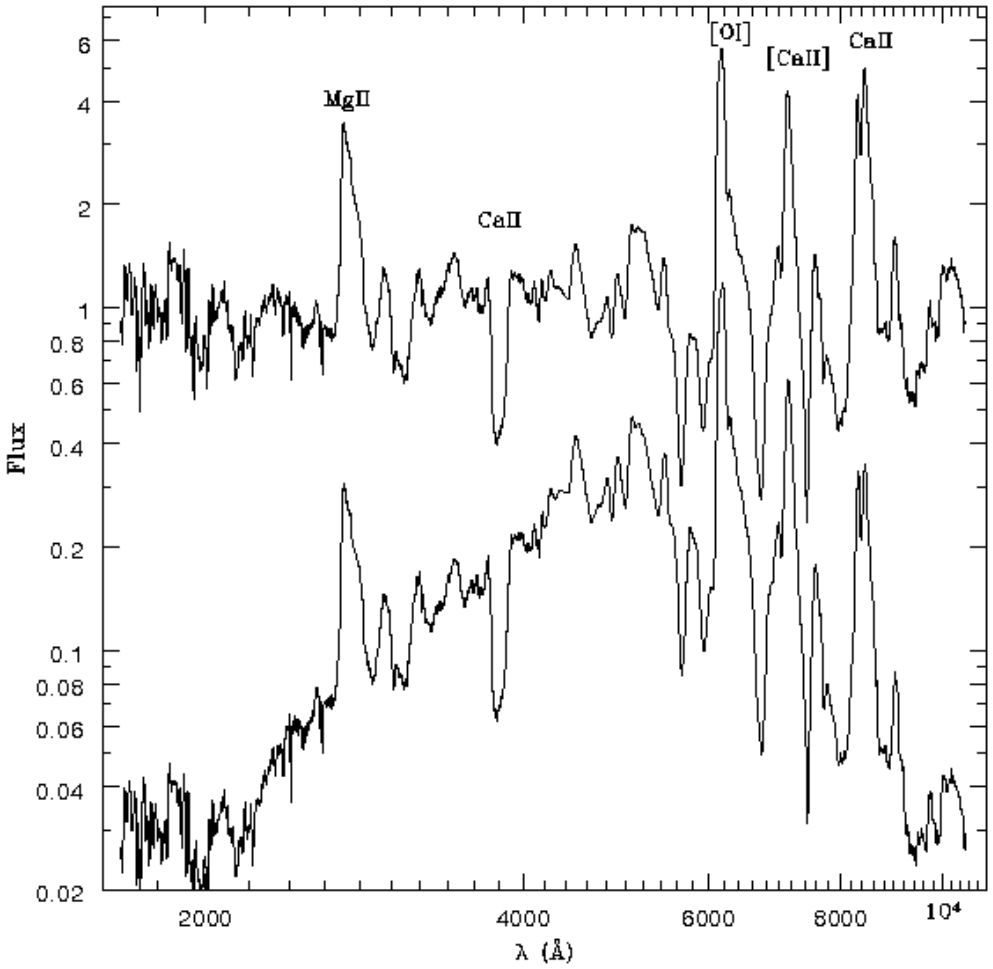

Fig. 3.— The spectrum of Type IIb SN 1993J in the f_λ and locally-normalized representations from 1993 September 15.5 (an averaged date) which is about 151 days after UVOIR bolometric maximum light and 171 days after explosion. From 4253.6 Å blueward, the spectrum is an *HST* spectrum (from 1993 September 17).

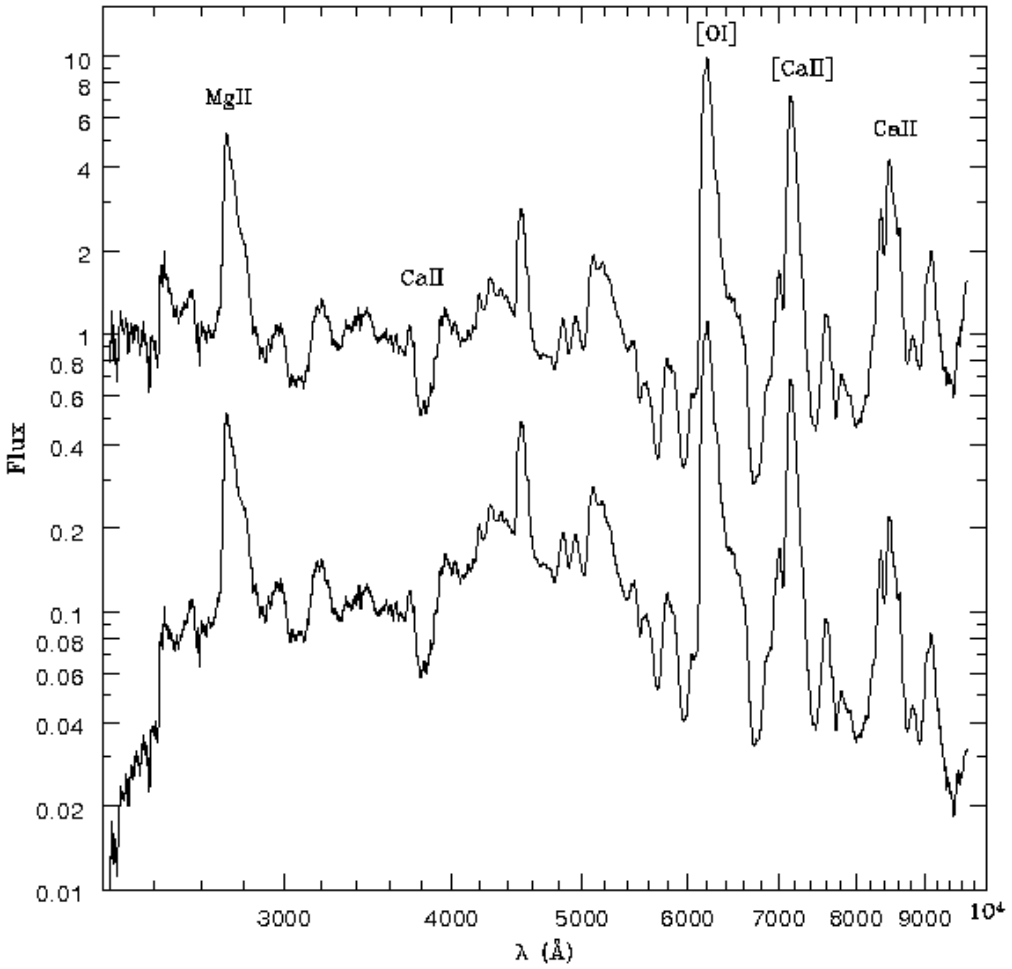

Fig. 4.— The spectrum of Type IIb SN 1993J in the f_λ and locally-normalized representations from 1993 November 15.5 (an averaged date) which is about 212 days after UVOIR bolometric maximum light and 232 days after explosion. From 4200 Å blueward, the spectrum is an *HST* spectrum (from 1993 November 14). The original *HST* spectrum blueward of ~ 2425 Å seems to decline in a manner too steep to be physically real and we do not trust it nor the locally-normalized spectrum there.

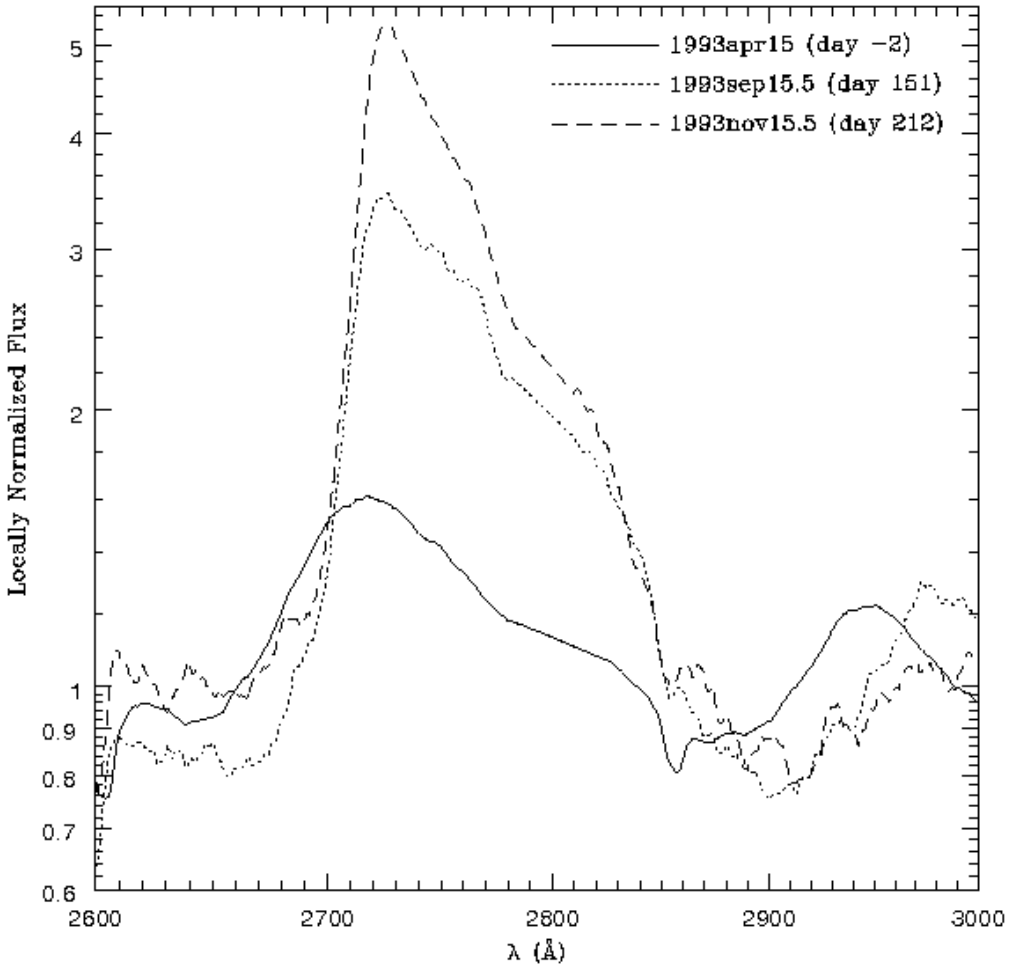

Fig. 5.— The evolution of the blueshifted Mg II λ2797.9 emission line in the locally-normalized spectra of SN 1993J. The phases given in parentheses in the figure are relative to the UVOIR bolometric maximum light on 1993 April 17. The horizontal axis is logarithmic, but this is hard to notice given the small wavelength range covered.

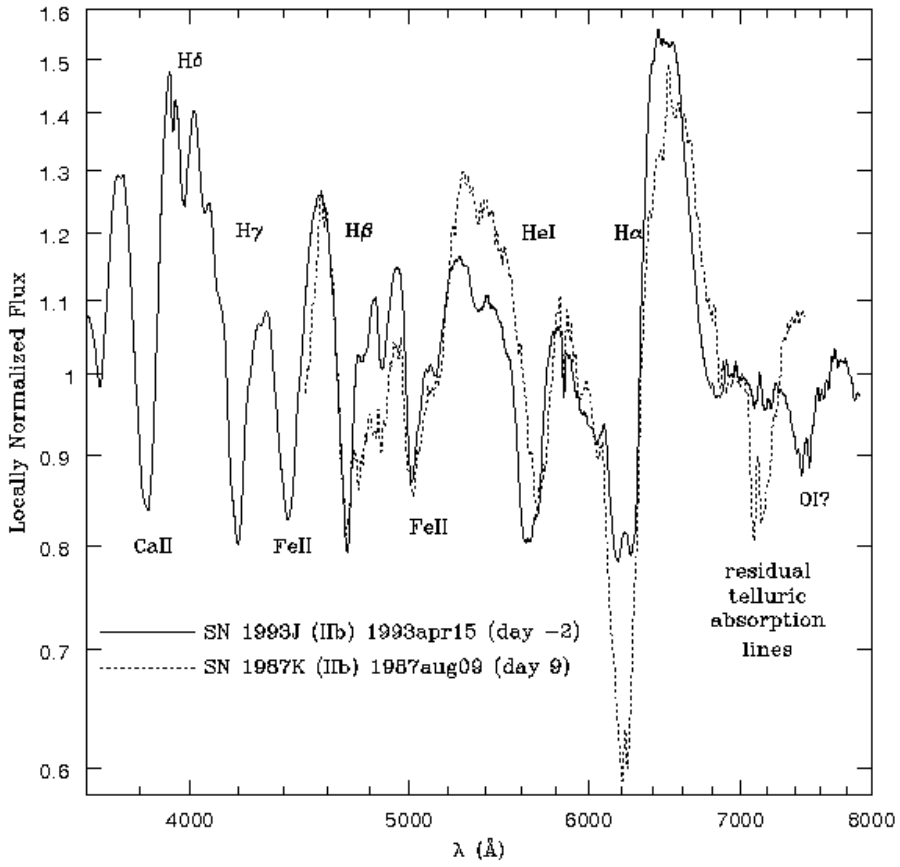

Fig. 6.— The locally-normalized spectra of Type IIb supernovae SN 1993J from 1993 April 15 (about 2 days before UVOIR bolometric maximum light) and SN 1987K from 1987 August 9 (about 9 days after a red-optical maximum light). The SN 1987K spectrum has been blueshifted using Doppler shift velocity parameter absolute value $999\,\mathrm{km\,s^{-1}}$ to minimize the DIFF2 function value for the spectrum pair. For the spectrum pair, DIFF1 = 0.642 and DIFF2 = 0.612. The spectra were both initially corrected for host galaxy heliocentric velocity: from Leda, the mean host galaxy heliocentric velocities are $-39 \pm 2\,\mathrm{km\,s^{-1}}$ (SN 1993J) and $799 \pm 2\,\mathrm{km\,s^{-1}}$ (SN 1987K) (Paturel et al. 2003).

Table 1. Current Sample in SUSPEND of HDCC Supernovae and Spectra

Type	Number of Supernovae	Number of Spectra
All HDCC Types	17	168
Type IIb	2	39
Type Ib/Ibc	8	45
Type Ic	4	34
Type Ic hyp	3	50

[a]Type Ibc supernovae are those supernovae which are not clearly distinguishable into Type Ib's or Type Ic's. We group Type Ib's and Type Ibc's together. There are only two Type Ibc' in the sample: SN 1999ex (Hamuy et al. 2002; Stritzinger et al. 2002) and SN 2005bf (e.g., Folatelli et al. 2006; Parrent et al. 2007). Type Ic hyp is short for Type Ic hypernovae.

Table 2. HDCC Supernova Type DIFF1/2 Correlation Matrix

Type\Type	Type IIb		Type Ib/Ibc[a]		Type Ic		Type Ic hyp[b]	
	Mean DIFF1/2	St.Dev.	Mean DIFF1/2	St.Dev.	Mean DIFF1/2	St.Dev.	Mean DIFF1/2	St.Dev.
(a) DIFF1: no phase restriction								
Type IIb	0.507	0.000	0.674	0.077	0.662	0.068	0.632	0.052
Type Ib/Ibc	0.674	0.077	0.615	0.097	0.646	0.113	0.712	0.081
Type Ic	0.662	0.068	0.646	0.113	0.578	0.118	0.614	0.085
Type Ic hyp	0.632	0.052	0.712	0.081	0.614	0.085	0.499	0.068
(b) DIFF2: no phase restriction								
Type IIb	0.507	0.000	0.644	0.071	0.618	0.038	0.601	0.042
Type Ib/Ibc	0.644	0.071	0.573	0.094	0.610	0.105	0.670	0.056
Type Ic	0.618	0.038	0.610	0.105	0.547	0.120	0.579	0.071
Type Ic hyp	0.601	0.042	0.670	0.056	0.579	0.071	0.455	0.020
(c) DIFF1: restricted to pre-10-days past maximum light								
Type IIb	0.507	0.000	0.730	0.064	0.699	0.066	0.735	0.086
Type Ib/Ibc	0.730	0.064	0.633	0.085	0.654	0.082	0.855	0.128
Type Ic	0.699	0.066	0.654	0.082	0.597	0.160	0.754	0.135
Type Ic hyp	0.735	0.086	0.855	0.128	0.754	0.135	0.504	0.072
(d) DIFF2: restricted to pre-10-days past maximum light								
Type IIb	0.507	0.000	0.696	0.053	0.647	0.038	0.681	0.069
Type Ib/Ibc	0.696	0.053	0.593	0.076	0.623	0.071	0.763	0.074
Type Ic	0.647	0.038	0.623	0.071	0.557	0.130	0.652	0.083
Type Ic hyp	0.681	0.069	0.763	0.074	0.652	0.083	0.485	0.064

[a]Type Ibc supernovae are those supernovae which are not clearly distinguishable into Type Ib's or Type Ic's. We group the Type Ib's and Type Ibc's together. There are only two Type Ibc's in the sample: SN 1999ex (Hamuy et al. 2002; Stritzinger et al. 2002) and SN 2005bf (e.g., Folatelli et al. 2006; Parrent et al. 2007).

[b]Type Ic hyp is short for Type Ic hypernovae.

Note. — This table gives the mean DIFF1/2 values between HDCC supernova types in a correlation matrix format. The DIFF1/2 value between two supernovae in this preliminary analysis is just defined to be the smallest DIFF1/2 value found out of all the pairs of spectra with one spectrum drawn from the one supernova and the other from the other supernova. With no phase restrictions the spectra are drawn from all phases. With phase restriction, the spectra are only drawn from the phases allowed by the given restriction. (The kind of maximum light used in setting the phase zero point is chosen various ways as discussed in § 5.1.) The matrix is symmetric, of course. The diagonal elements are the mean DIFF1/2 values for pairs with supernovae of the same type in the pairs: we call these means the self-type means. The off-diagonal elements are the mean DIFF1/2 values for pairs with supernovae of different types in the pairs: we call these means the cross-type means. More digits are shown than are significant to allow for numerical consistency checks and to give the table a consistent appearance.